ÅBO AKADEMI

INSTITUTIONEN FÖR KEMITEKNIK

DEPARTMENT OF CHEMICAL ENGINEERING

Processkemiska centret

Process Chemistry Centre

REPORT 13-01

Oxidation rates of carbon and nitrogen in char residues from solid fuels

Oskar Karlström

Doctoral Thesis

Laboratory of Inorganic Chemistry

Oxidation rates of carbon and nitrogen in char residues from solid fuels

Oskar Karlström

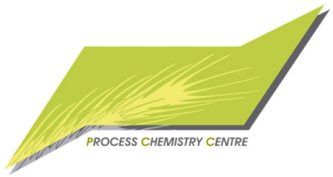

Doctoral Thesis

Laboratory of Inorganic Chemistry
Process Chemistry Centre
Department of Chemical Engineering
Åbo Akademi University
2013

Supervisors
Docent Anders Brink
Åbo Akademi University

Professor Mikko Hupa
Åbo Akademi University

Opponent
Professor Kim Dam-Johansen
Technical University of Denmark

Reviewers
Professor Henrik Thunman
Chalmers University of Technology

Docent Jaakko Saastamoinen
University of Jyväskylä

ISSN 159-8205
ISBN 978-952-12-2891-9 (paper version)
ISBN 978-952-12-2892-6 (pdf version)
Painosalama Oy
Åbo, Finland, 2013

Preface

The present work was carried out at the Laboratory of Inorganic Chemistry, Department of Chemical Engineering, Åbo Akademi University between 2008 and 2013. The research is a part of the activities performed at Åbo Akademi Process Chemistry Centre. The research was partly funded by the Nordic Gaduate School of Biofuel Science and Technology and by the two projects Chemcom 2 and Fusec. These projects were financially supported by the National Agency of Finland (Tekes), Andritz Oy, Foster Wheeler Energia Oy, International Paper Inc, Metso Power Oy, Oy Metsä Botnia Ab, Clyde Bergemann GmbH, UPM-Kymmene Oyj, and Top Analytica Oy Ab. Further the research has been funded by the ERANET-Bioenergy project SciToBiCom and by the project Symbiosis with financing from the Academy of Finland.

I would like to thank Docent Anders Brink and Professor Mikko Hupa for their professional supervision during this thesis. I have had scientific discussions with Anders almost every week during my thesis. In simple or complex scientific questions, his help has been very valuable. He has had the enthusiasm to always provide help within a very reasonable time, no matter how many scientific or industrial projects he has been involved in.

I am very happy that I have had the opportunity to work under Professor Hupa. During my thesis I have had many scheduled and spontaneous meetings with him. Regardless of the quality of my scientific research ideas or problems I have presented for Mikko, his first impression has always been positive and characterized by curiosity. He is a master in understanding complex scientific problems from other people's point of view. This in combination with his high pedagogic skills and his knowledge to attach scientific problems from various angels has had a strong influence on the quality of my research.

I would also like to thank Professor Leonardo Tognotti for giving me the opportunity to take part in the activities at the International Flame Research Foundation (IFRF) in Livorno, Italy. I am grateful that Professor Hupa and Professor Tognotti gave me the opportunity to work with the IFRF solid fuel data base from which I have used a significant amount of experimental data

within this thesis. As part of this collaboratory, I have had the opportunity to visit IFRF in Livorno several times during my thesis. As a result of these visits I have gotten a good picture regarding how IFRF works and how/why research should be performed and shared internationally.

During my thesis I have participated in industrial project meetings and scientific seminars and attended high quality scientific conferences in Finland, Europe, China and the US. Two times I have participated at the International Symposium of Combustion, 2010 in China and 2012 in Poland. Both times our full scale journal papers were accepted for presentation; only around 400 of 1100 submitted full-scale scientific papers were accepted for the conferences. This would not have been possible without the help from Brink, Tognotti, and Hupa.

It has been very inspiring to work at the Laboratory of Inorganic Chemistry within the Process Chemistry Centre (PCC) at Åbo Akademi University. At PCC we are around 130 persons of around 22 different nationalities. I believe that I have had discussion with researchers and persons from nearly all these countries. This has given me many fun moments and a multicultural perspective.

Finally I would like to thank my parents, Kirsti and Rune, for all their support during this thesis and during my entire life.

Abstract

Computational fluid dynamics (CFD) modeling is an important tool in designing new combustion systems. By using CFD modeling, entire combustion systems can be modeled and the emissions and the performance can be predicted. CFD modeling can also be used to develop new and better combustion systems from an economical and environmental point of view. In CFD modeling of solid fuel combustion, the combustible fuel is generally treated as single fuel particles. One of the limitations with the CFD modeling concerns the sub-models describing the combustion of single fuel particles. Available models in the scientific literature are in many cases not suitable as sub-models for CFD modeling since they depend on a large number of input parameters and are computationally heavy.

In this thesis CFD-applicable models are developed for the combustion of single fuel particles. The single particle models can be used to improve the combustion performance in various combustion devices or develop completely new technologies. The investigated fields are oxidation of carbon (C) and nitrogen (N) in char residues from solid fuels.

Modeled char-C oxidation rates are compared to experimental oxidation rates for a large number of pulverized solid fuel chars under relevant combustion conditions. The experiments have been performed in an isothermal plug flow reactor operating at 1123-1673 K and 3-15 vol.% O_2. In the single particle model, the char oxidation is based on apparent kinetics and depends on three fuel specific parameters: apparent pre-exponential factor, apparent activation energy, and apparent reaction order. The single particle model can be incorporated as a sub-model into a CFD code. The results show that the modeled char oxidation rates are in good agreement with experimental char oxidation rates up to around 70% of burnout. Moreover, the results show that the activation energy and the reaction order can be assumed to be constant for a large number of bituminous coal chars under conditions limited by the combined effects of chemical kinetics and pore diffusion. Based on this, a new model based on only one fuel specific parameter is developed (Paper III). The results also show that reaction orders of bituminous coal chars and anthracite chars differ under similar conditions (Paper I and Paper II); reaction orders of bituminous coal chars were found to be one, while reaction orders of anthracite chars were determined to be zero.

This difference in reaction orders has not previously been observed in the literature and should be considered in future char oxidation models. One of the most frequently used comprehensive char oxidation models could not explain the difference in the reaction orders. In the thesis (Paper II), a modification to the model is suggested in order to explain the difference in reaction orders between anthracite chars and bituminous coal chars.

Two single particle models are also developed for the NO formation and reduction during the oxidation of single biomass char particles. In the models the char-N is assumed to be oxidized to NO and the NO is partly reduced inside the particle. The first model (Paper IV) is based on the concentration gradients of NO inside and outside the particle and the second model is simplified to such an extent that it is based on apparent kinetics and can be incorporated as a sub-model into a CFD code (Paper V). Modeled NO release rates from both models were in good agreement with experimental measurements from a single particle reactor of quartz glass operating at 1173-1323 K and 3-19 vol.% O_2. In the future, the models can be used to reduce NO emissions in new combustion systems.

Referat på svenska

CFD-modellering (engelska: Computational Fluid Dynamics, svenska: numerisk strömningsdynamik) är ett centralt verktyg vid utveckling av förbränningsanläggningar. Genom att använda CFD-modellering kan utsläppen och prestandan för förbränningskraftverk förutspås. CFD-modellering kan även användas till att utveckla nya förbränningsteknologier med högre prestanda och lägre utsläpp än i befintliga förbränningsanläggningar. Vid förbränningsmodellering av fast bränsle kan det brännbara materialet betraktas som ett stort antal bränslepartiklar. Partikelmodeller som beskriver förbränningsförloppet för enskilda bränslepartiklar är kritiska för CFD-modelleringen. Tillgängliga modeller i den vetenskapliga litteraturen kan i många fall inte tillämpas i CFD-modellering eftersom de beror på ett stort antal modellparametrar och kräver långa numeriska beräkningstider.

I denna avhandling utvecklas modeller för förbränningen av enskilda bränslepartiklar som kan användas som partikelmodeller i CFD. Modellerna kan både användas vid förbättrandet av befintliga förbränningsanläggningar och för utvecklandet av nya förbränningsteknologier. Förloppen som studeras är oxidation av kol (C) och kväve (N) i koksrester från fasta bränslen.

Reaktionshastigheter för C-oxidation från enstaka kokspartiklar har modellerats och studerats experimentellt i en isoterm pluggflödesreaktor. Experimenten utfördes vid 1123-1673 K och 3-15 vol.% O_2. Partikelmodellen som använts baserar sig på observerbar kinetik och är beroende av tre bränslespecifika parametrar: frekvensfaktor, aktiveringsenergi och reaktionsordning. Resultaten visar att såväl aktiveringsenergin som reaktionsordningen är oberoende av kokstyp för ett stort antal bituminösa kolsorter. Utgående från detta utvecklas en ny modell som endast baserar sig på en bränslespecifik parameter. Resultaten visar även att reaktionsordningen skiljer sig för koks från bituminösa kol och antracit. Skillnaden i reaktionsordningar har tidigare inte observerats i den vetenskapliga litteraturen och är av stor vikt för att för att förstå reaktionen mellan syre och koks-C under förbränningsförhållanden. I avhandlingen visas att en av de mest använda modellerna i den vetenskapliga litteraturen inte förmår förklara den observerade skillnaden i reaktionsordningen. I avhandlingen utvecklas en ny modell som kan förklara skillnaden i reaktionsordningen.

I avhandlingen utvecklas även två partikelmodeller för utsläppen av kväveoxid (NO) under koksförbränningsskedet av fast biomassa. Den första modellen är detaljerad och tar explicit i beaktande produktion och diffusion av NO i och utanför partikeln. Den andra modellen är förenklad till den grad att den är tillämplig för CFD-modellering. Förenklingarna i den andra modellen motiveras utifrån resultat från den första modellen. Den utvecklade modellen för NO-utsläpp är den första i sitt slag som kan användas i CFD-modellering. I avhandlingen jämförs modellerade NO utsläpp från båda modellerna med experimentellt bestämda NO utsläpp från en reaktor för enstaka biomassapartiklar. Experimenten är utförda vid 1073-1323 K och 3-19 vol.% O_2. Båda modellerna förutspår de experimentellt bestämda NO-utsläppen med god noggrannhet; NO utsläppen ökar som funktion av minskad partikeldiameter och partikelmassa. Modellerna kan i framtiden användas för att minska kväveutsläppen i nya förbränningsanläggningar.

Contents

1. Context and objectives of thesis

1.1 Context

Solid fuel combustion continues to be one of the most important sources for the generation of energy and power. Today solid fuel combustion accounts for around 40% of the global electricity supply [1]. In combustion units the trends are to achieve higher efficiencies with lower emissions. Moreover, the trends are to burn a larger variety of fuels and more complicated fuels in terms of combustion performance and harmful emissions. To achieve these goals various tools have been used in order to improve the design of combustion systems. One such tool is computational fluid dynamics (CFD) modeling. In CFD modeling of solid fuel combustion, the furnace is divided into a large number of cells forming a computational grid. Within the grid mass, momentum, energy and species balances are solved simultaneously. Fig. 1 illustrates one example of CFD modeling of solid fuel combustion [2].

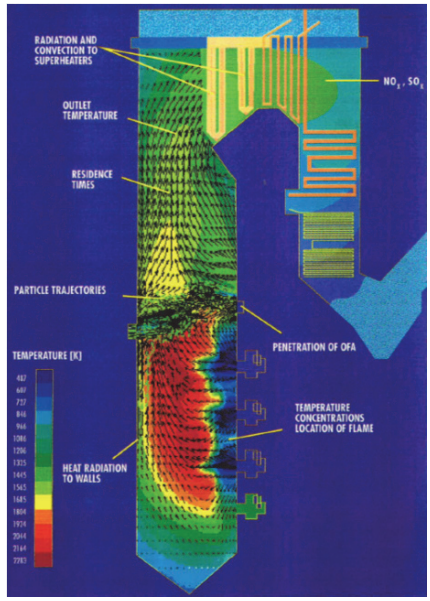

Fig. 1. CFD modeling of solid fuel combustion.
Taken with permission from reference [2].

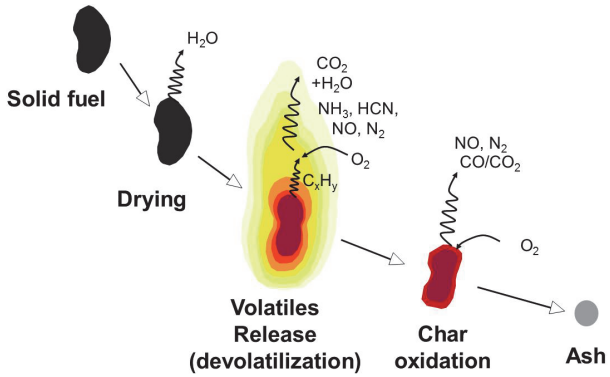

Fig. 2. Combustion stages of a fuel particle.

By using CFD modeling, entire combustion systems can be modeled and the performance and emissions can be predicted. CFD modeling can also be used to develop new and better combustion systems from an economical and environmental point of view. In many cases the CFD modeling relies on sub-models describing the conversion of single fuel particles. Fig. 2 illustrates the conversion stages of a single fuel particle in a combustion environment. The conversion stages can be divided into drying, devolatilization, and char oxidation.

Models for the conversion stages are available in the scientific literature, but in many cases the models are not suitable as sub-models for CFD modeling since they are computationally heavy and require a large number of input parameters. Two fields where there is no consensus regarding the type of sub-models that should be used are the oxidation of carbon (C) and nitrogen (N) in the char. Sub-models for char-C and char-N oxidation are vital for CFD modeling of combustion systems. For example, in the design of a new combustion system, CFD modeling with an appropriate sub-model for the char-C oxidation provides information on whether the size of the system is sufficient, whether the carbon content in the residual ash is sufficiently low, and whether temperatures are acceptable. Correspondingly, a char-N oxidation sub-model provides important information regarding the harmful NO release.

1.2 Objectives of thesis

The objectives of this thesis were to get a better insight in the details of char oxidation and to develop new char oxidation sub-models that can be incorporated into CFD codes for combustion systems. With such models it is possible to improve the combustion performance in various combustion devices or to develop completely new technologies.

1.3 List of publications

I. O. Karlström, A. Brink, M. Hupa, L. Tognotti. Multivariable optimization of reaction order and kinetic parameters for high temperature oxidation of 10 bituminous coal chars. Combustion and Flame 158 (2011) 2056-2063

II. O. Karlström, A. Brink, E. Biagini, M. Hupa, L. Tognotti. Comparing reaction orders of anthracite chars with bituminous coal chars at high temperature oxidation conditions. Proceedings of the Combustion Institute 34 (2013) 2427-2434

III. O. Karlström, A. Brink, J. Hercog, M. Hupa, L. Tognotti. One-parameter model for the oxidation of pulverized bituminous coal chars. Energy and Fuels 26 (2012) 968-975

IV. O. Karlström, A. Brink, M. Hupa. Biomass char nitrogen oxidation - single particle model. Energy and Fuels 27 (2013) 1410-1418

V. O. Karlström, A. Brink, M. Hupa. Time dependent production of NO from combustion of large biomass char particles. Fuel 103 (2012) 524-532

1.4 Contribution of author

I-III. The author developed the models and the optimization routines. The author selected the data from the IFRF solid fuel data base. The author was responsible for the evaluation of the results and was the main author of the papers.

VI-V. The author planned the experiments, performed the experiments, and developed the models and the optimization routines. The author was responsible for the evaluation of the results and was the main author of the papers.

2. Introduction

A solid fuel particle that is introduced to a hot combustion environment dries and devolatilizes forming a residual char. The residual char is oxidized and finally an ash residue remains. Fig. 3 shows the combustion of a wood particle at 1000 °C and 19 vol.% O_2 in a laboratory scale reactor. The spherical particle is attached on a platinum wire. After the drying the devolatilization starts and the particle becomes surrounded by a visible flame. As the volatile matter has released the flame disappears and the char oxidation begins. The residual char consists an organic part and of an inorganic part. For coals, the char content varies between around 30-95% of the original fuel on dry and ash free basis. For wood the char content is around 15% on a dry and ash free basis. The organic part of the char consists of carbon, hydrogen, nitrogen, sulfur, and oxygen. In this thesis, oxidation of carbon (C) and nitrogen (N) in the char is investigated. In chapter 2.1 oxidation of char-C is introduced and in chapter 2.2 oxidation of char-N is introduced.

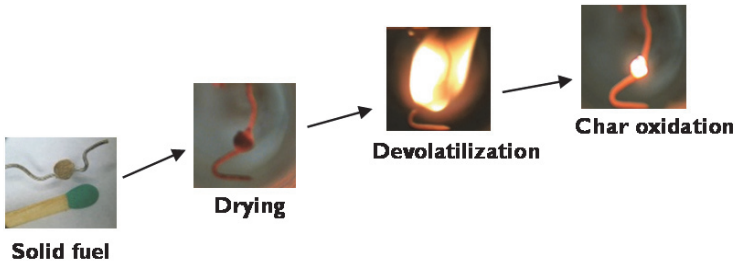

Fig. 3. Combustion of a wood particle attached on a platinum wire in a laboratory scale reactor.

2.1 Char-C oxidation

Numerous studies are available in the literature on char-C oxidation. In *Chemistry of Coal Utilization* (1980) [3] Essenhigh lists 38 review studies on the combustion of coal particles. Several review studies have appeared also on the thermal conversion of biomass [e.g. 4-7]. In the oxidation of char-C by oxygen, a series of intermediate reaction occurs, and the final primary products are CO and CO_2. The product ratio depends on the temperature since the activation

energies of the reactions differ [8,9]. Further, the product ratio depends on the concentration of oxygen [10]. In general, the CO_2/CO-product ratio is believed to decrease as a function of increasing temperature [8,9]. At 1000 K, 70-90% of the char-C is expected to react to CO and at 1600 K, more than 90% of the char-C is expected to react to CO [10]. Fig. 4 shows predicted and experimental CO_2/CO product ratios for coal chars at various temperatures [10]. It can be seen that the product ratio increases both with decreasing temperature and with increasing oxygen concentration in the gas phase. With a higher oxygen concentration the coverage of chemisorbed oxygen atoms increases. This influences the rate limiting mechanisms in such way that the role of the CO_2 forming reaction steps increases.

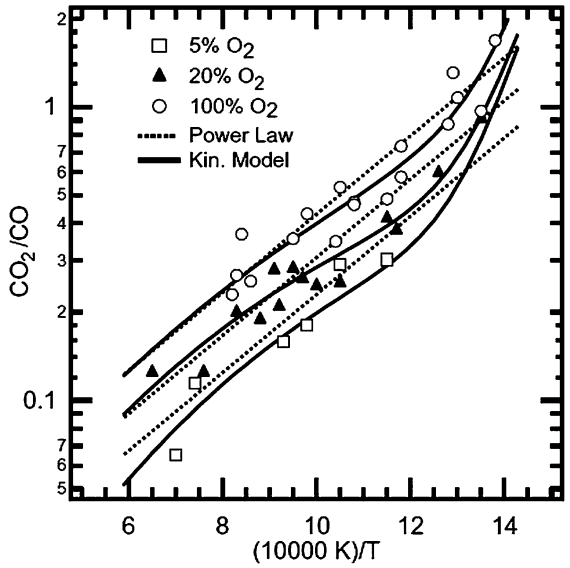

Fig. 4. Experimental (symbols) and modeled CO_2/CO ratios as a function of inverse temperature. Taken with permission from reference [10].

Char particles are normally porous in such way that the oxygen is allowed to diffuse inside the particle. If a char particle is very small and the reaction rate is low, the concentration of oxygen is uniform in the entire particle. In such a case, the reaction rate is limited by chemical kinetics. In the combustion literature this is generally called Regime I conditions.

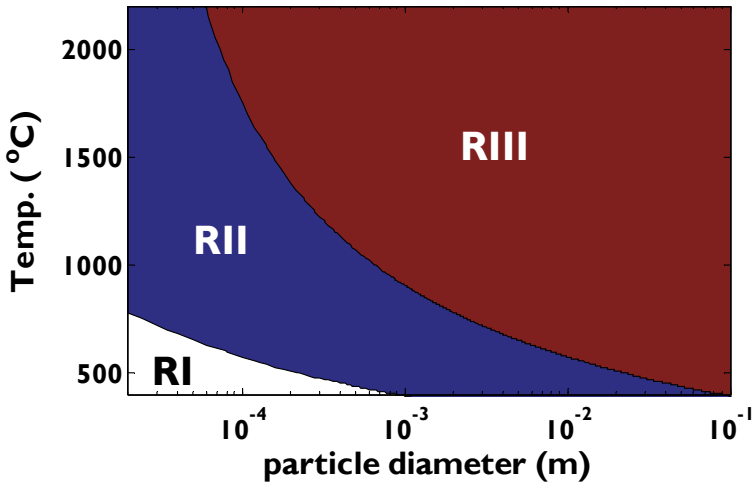

Fig. 5. Regime I, Regime II, and Regime III conditions for char-C oxidation of a coal particle. Figure by the author.

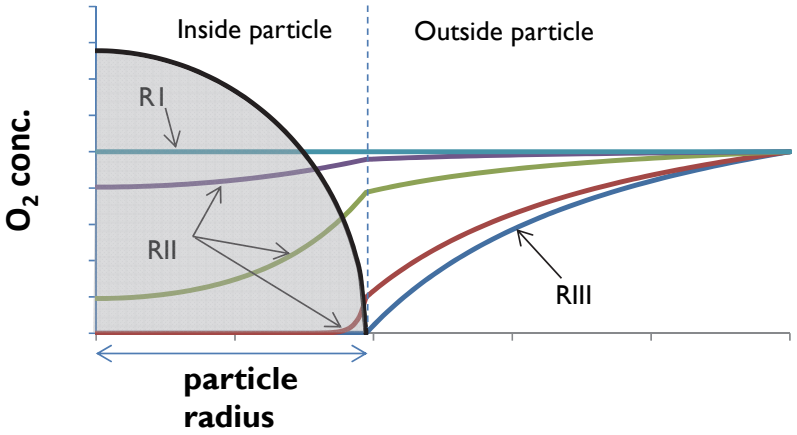

Fig. 6. Oxygen concentration profiles inside and outside a char particle under Regime I, Regime II, and Regime III conditions. Figure by the author.

If a char particle is large and the temperature is high, the oxygen is consumed very close to the external surface of the char particle. The penetration depth of oxygen and the external surface concentration of oxygen approaches zero. Under such Regime III conditions, the reaction rate is limited by external mass transfer of oxygen. In the intermediate region, i.e., Regime II conditions,

the reaction rate is limited by the combined effects of chemical kinetics and diffusion of oxygen. Areas for the regimes are illustrated in Fig. 5 for one coal char. This figure is plotted based on a concept called Thiele-modulus which is briefly discussed in chapter 4.2.2. The limits for these areas are strongly dependent on the char type. Biomass char particles, for example, are generally significantly more reactive than coal chars with respect to O_2 and as a result a lower temperature is required for a biomass char particle to be oxidized under Regime III conditions than for a coal char particle.

Fig. 6 shows concentration profiles of oxygen inside and outside a char particle under the three regimes. Under Regime III conditions, the concentration of oxygen is zero in the entire particle except for very close to the external surface of the particle. On the other hand, the oxygen concentration is uniform in the entire particle under Regime I conditions due to slow char oxidation reactions in comparison to the transport of oxygen. Under Regime II conditions, the oxygen concentration inside the particle is characterized by gradients. The penetration depth of oxygen varies from a small fraction of the particle radius to the entire particle radius.

Fig. 7 exemplifies the size evolution of a spherical particle under the three regimes. Under Regime I conditions, the reactions occur in the entire particle. As a result the external diameter is constant and the density decreases as a function of char conversion. Under Regime III conditions the char is consumed very close to the external surface. Consequently, the density of the char core is almost constant during the entire conversion. Dependent on the penetration depth of oxygen, the diameter development differs under Regime II conditions. If the penetration depth is small, the density of the char particle is relatively constant as a function of conversion and vice versa. In real combustion systems, the same particle can be oxidized under several regimes. For example, the char oxidation may begin under Regime II conditions and as the particle decreases in size, the oxidation conditions changes to Regime I conditions. In real combustion systems the analysis of the oxidation regimes is also complicated by the fact that various particles may burn under different regimes. In pulverized fuel combustion, for example, there is usually a significant distribution of particle sizes. Small particles of 1 μm may be oxidized under Regime I conditions, while larger particles of 100 μm may burn under Regime II conditions or Regime III conditions.

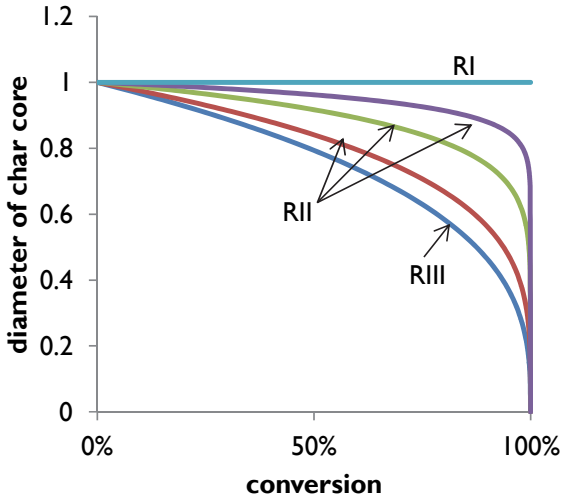

Fig. 7. Development of diameter during oxidation of a char particle under Regime I, Regime II, and Regime III conditions. Figure by the author.

Under Regime III conditions, the char oxidation rate can be predicted by Ficks´ law. In such cases the char oxidation rate can be predicted if the temperature, bulk concentration of oxygen, the CO/CO_2 product ratio, and the external size and shape is well defined. To predict char-C oxidation rates of char particles under Regime I and Regime II conditions, various models based on intrinsic kinetic or apparent kinetics are generally used [7,11]. In the intrinsic kinetic models, the char oxidation rate is related to the internal surface area of the particle. The internal surface area, as well as the fraction of the internal surface area, that participates in the heterogeneous reactions, changes throughout the char conversion [9,12]. The internal surface area of the initial char particle depends on various factors such as internal surface area of parent fuel, the volatile content and the heating rate. For example, if the volatile content is high and the heating rate is high, the pores open up which may result in a high internal surface area [3]. Further, the development of the internal surface area depends on the initial internal surface area of the char and on the pore size distribution. Since all these factors must be considered it is complicated to predict the development of the internal surface area under Regime I conditions. Under Regime II conditions it is even more complicated to take into account the evolution of the internal surface area, since only a fraction of the entire surface area may undergo a development at a given time [13]. Partly because of this, models based on apparent kinetics are widely used. In models based

on apparent kinetics the char oxidation rate is related to the mass or to the external surface area of the particle. Further, the char oxidation is related to the bulk or surface concentration of oxygen and concentration gradients of oxygen inside the particle are not taken into account explicitly as for intrinsic models. Taking into account particle size distribution and deactivation of the char, models based on apparent kinetics can, however, accurately predict char combustion at early, intermediate, and late combustion stages [14-18]. Moreover, such models rely on a smaller number of fuel specific parameters than models based on intrinsic kinetics. Therefore, the models are attractive for CFD modeling.

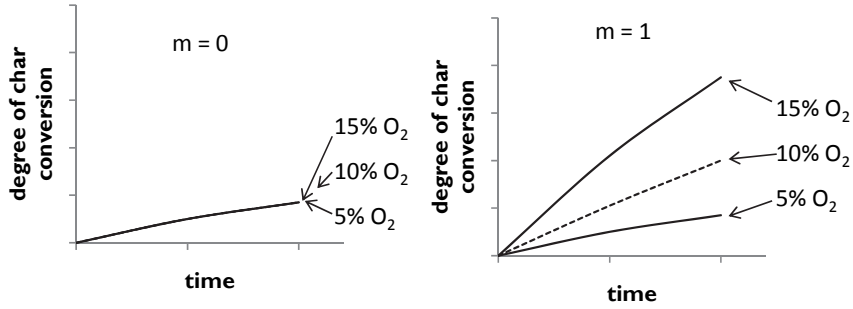

Fig. 8. Fractional degree of char conversion with various oxygen concentrations and reaction orders. Figure by the author.

In order to use models based on intrinsic or apparent kinetics, the reaction order must be defined. Fig. 8 shows char conversion as a function of time with various oxygen concentrations in the bulk phase and using reaction orders of zero and one. The figure illustrates the influence of the reaction order on the char oxidation rate. At a given char particle temperature, the char oxidation rate is not influenced by an increased oxygen concentration in the gas phase using a reaction order of zero. Contrary, the char oxidation rate is strongly dependent on the oxygen concentration using a reaction order of one.

Under Regime I conditions, true reaction orders have been determined to be zero for coal chars [19], while most of the studies in contrast report a high fractional reaction order at the same conditions [20,21]. Under Regime II conditions, reaction orders have been reported to be one for various chars [22,23]. On the other hand, it has frequently been stated that the true reaction order is near zero at these conditions [21]. At very high temperatures and for large char particles, the

oxidation rates are controlled by external diffusion, i.e., Regime III conditions. At these conditions the reaction order can be expected to be one. However, at near external diffusion limited conditions the apparent reaction order has been reported to be 0.1 [18]. This is in contrast to the frequently used correlation $n = (m+1)/2$, where m is the true reaction order and n is the apparent reaction order. It is thus obvious that there is no consensus regarding the reaction order of coal chars neither at Regime I nor at industrially relevant Regime II conditions.

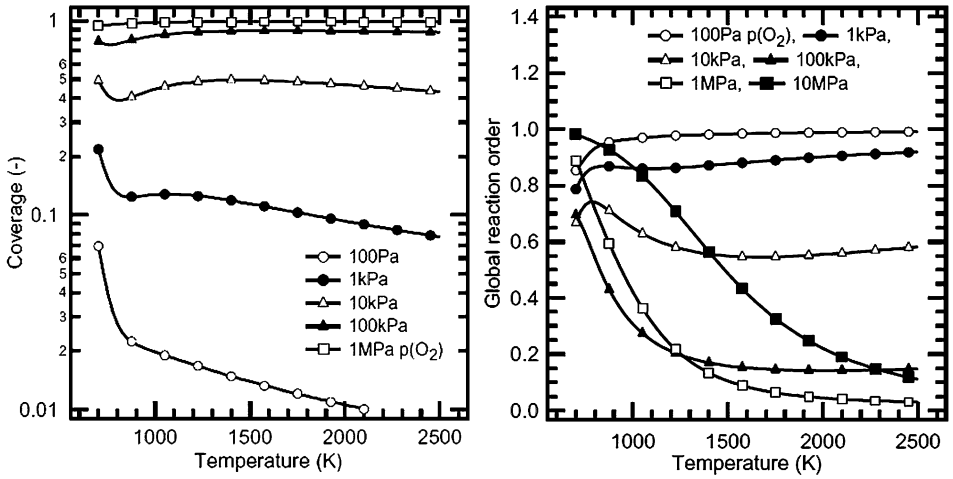

Fig. 9. Predicted coverage and reaction order as a function of temperature. Taken with permission from reference [10].

The char type influences the reaction order, since catalytic effects influence the rate limiting mechanisms of the char oxidation [24,25]. Moreover, the internal surface area influences the reaction order: if the internal surface area increases under Regime II conditions, the partial pressure of oxygen decreases inside the char particle. In such a case, the coverage of chemisorbed oxygen atoms changes and may result in changed rate limiting mechanisms and reaction orders. Fig. 9, taken from a study of Geier et al. [10], shows that, for example, at 1500 K the local coverage can vary from 0.1 to 1 and the corresponding intrinsic reaction order vary in the range between 1 to 0.1. Few studies, however, report on the impact of the char type on the reaction order at high temperatures. Smith suggested that the apparent reaction order for pulverized anthracite chars, bituminous coal chars, and petroleum coal chars is one in the temperature interval 1200 to 2270 K [23]. Field [22] reported reaction orders of one for 11 chars of various

coal rank at 1200–2270 K. However, the objectives of these studies were to investigate the overall reactivity, rather than to determine the correct reaction orders. On the contrary, Hurt and Calo [21] reported that intrinsic reaction orders generally have been determined to be zero in the temperature interval 1200 to 1700 K. In the studies the influence of the char type on the reaction order has not been investigated. To evaluate the extent to which the char type influences the reaction order two types of investigations must be carried out: (i) reaction orders of similar types of chars, i.e., rank and size, should be determined under the same conditions; and (ii) this comparison should be repeated for chars of various coal ranks.

In this thesis (**Paper I**) reaction orders are determined for the oxidation of 10 bituminous coal chars. Modeled char oxidation rates are compared to experimental measurements obtained from an isothermal plug flow reactor operating (IPFR) at 1223 K and 4-12 vol.% O_2. The reaction orders are determined using a parameter optimization approach recently suggested by Murphy and Shaddix [18]. In their work and also in the work by Ballester and Jimenez [17] it was suggested that conventional Arrhenius plots cannot be used to determine kinetic parameters for char oxidation under regime II conditions. Paper I of this thesis was the first study to apply the parameter determination methods suggested by Murphy and Shaddix [18] for a large number of coal chars. Further in this thesis (**Paper II**) reaction order of 5 anthracite chars are determined by using the same parameter optimization method. The reaction orders of the anthracite chars and of the bituminous coal chars are discussed in light of semi-global intrinsic char oxidation mechanisms.

Besides the reaction order, apparent kinetic models are dependent on the apparent pre-exponential factor and the apparent activation energy. The pre-exponential factor, A_a, includes effects of pore diffusion and of the internal surface area. The apparent activation energy, E_a, describes the char oxidation rate dependence on the temperature. While the pore diffusion effects are not explicitly included in the apparent kinetic model, E_a differs from the intrinsic activation energy, E_i. Under Regime II conditions, it has been suggested that the value of E_a is about half of the value of E_i [11,26]. The relationship $2E_a \approx E_i$ can be shown for simple particle shapes [27]. In general, E_a-values have been determined to be around 50-100 kJ/mol, and E_i values are around 100-200 kJ/mol [e.g. 3,4,7,11,17,18,21,22,28-31] under Regime II conditions. Fu et al. [8],

suggested E_i to be independent on the parent coals properties. They showed that calculated kinetic rates of bituminous coal chars and anthracite chars were relatively similar to experimentally determined rates by using a constant E_i. They emphasized that E_i is affected mainly by chemical factors, such as carbon type, active sites, and catalytic effects that have similar influences both on bituminous coal char and anthracite chars. For lignite chars, the mineral matter has an important influence on E_i, which therefore differs from E_i of bituminous coal chars and anthracite chars [24,25]. However, physical factors influencing the oxidation rates are char specific, also for chars derived from parent coals of similar rank. Therefore, although E_i may be the same for a various coal chars it is unclear whether E_a can be assumed to be constant, since E_a depends on physical factors and of the particle shape.

In this thesis (**Paper III**) char oxidation rates of 22 bituminous coal chars are modeled by separately optimizing E_a for each char and with a constant E_a for all the chars. Modeled rates were compared to experimental rates determined from the IPFR at 1123-1673 K and 3-15 vol.% O_2.

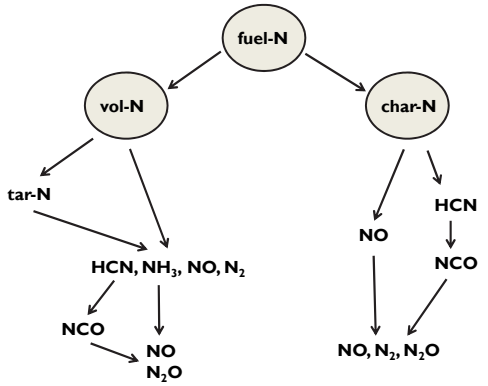

Fig. 10. Simplified conversion path of fuel bound nitrogen during solid fuel combustion.Re-plotted from reference [40].

2.2 Char-N oxidation

The organically bound nitrogen in the fuel is released during the devolatilization and during the char oxidation. Fig. 10 shows a simplified scheme of the pathways of nitrogen during devolatilization and char oxidation. In this section the devolatilization is not considered and the focus is thus on the char oxidation part.

During the oxidation of a solid char particle, the oxidation of carbon and nitrogen is frequently assumed to be non-selective [32-35], with a few exceptions [36,37]. By assuming this non-selectivity, the rate of char-N oxidation can be obtained from the rate of carbon oxidation and the N/C ratio in the char. Under Regime II conditions, char-C oxidation rates can be obtained by using intrinsic or apparent kinetic models as described in section 2.1. For larger char particles being oxidized e.g. under fluidized bed conditions, the char-C oxidation may occur under Regime III conditions although the temperatures are significantly lower than in pulverized fuel combustion. Under such conditions, the char-C oxidation can be modeled assuming Fick´s law.

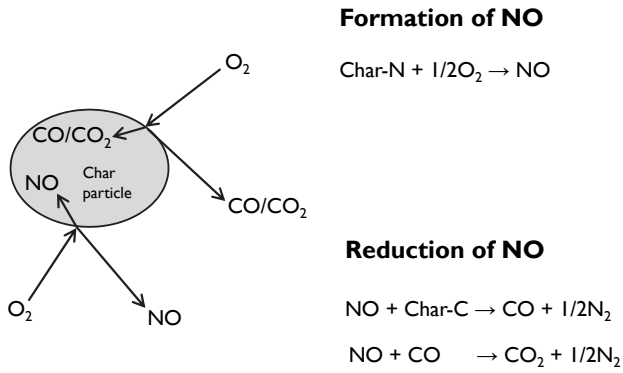

Fig. 11. Formation and reduction of NO inside a char particle.
Figure by the author.

A number of products have been observed from char-N oxidation: e.g. NO, N_2O, HCN, NH_3, HNCO, and N_2 [38]. During the combustion of char particles of both coal and biomass, the main reaction product can, however, be assumed to be NO [32,38-40]. The NO initially formed during the char-N oxidation is partly reduced inside the char particle. Fig. 11 illustrates the initial formation and reduction by NO inside a char particle. Although the NO may be initially formed close to the external surface of the particle, the NO can partly diffuse inside the particle and undergo reduction reactions. The most important reductions are NO-char reactions and surface catalyzed NO-CO reactions as the NO diffuses inside the particle. The fraction of the initially formed NO reduced inside a char particle decreases as functions of char conversion and decreasing particle size [41-43]. In gas atmospheres containing NO, addition of CO has been

reported to increase the NO reduction rates both for biomass chars [44] and for coal chars [45,46]. Contrary, for peat char it has been shown that NO reduction rates decreased by CO addition in the gas [44]. In general, the relative importance of these reduction reactions is not well understood under combustion conditions [45]. The reduction reactions are also influenced by catalytic elements, but there is no general agreement on the quantitative importance of catalytic elements on reactions between NO and char-C [46].

In experiments carried out to investigate the reduction of NO inside char particles, char particles are generally introduced to a gas with a known background level of NO [46]. In such experiments, the reduction rate of NO can be related to the concentration of NO in the gas bulk phase and to the instantaneous mass of the char or to the internal surface area of the char [46]. In the char-NO review study by Aarna and Suuberg [46] it is shown that at e.g. 1250 K, reaction rate constants on surface area basis for the reaction of NO with coal chars vary by more than three orders of magnitude. At temperatures between 673 and 1250 K and NO pressures between 0.03-0.65 kPa, activation energies vary between 43 and 196 kJ/mol and reaction orders vary between 0.22 and 1 [46]. For a large number of chars, it is shown that there is no consistent variation of activation energy with rank, surface area, or partial pressure of NO. Moreover it is suggested that coal chars are more reactive for NO reduction than highly ordered and/or highly heat treated carbons.

In order to predict the reduction of NO inside a char particle under combustion conditions the concentration profile of NO inside the particle must be taken into account. Studies taking into account the intra-particle concentration profile of NO are available both for fluidized bed [42,43,48] and for pulverized fuel combustion conditions [49,50] for coal char particles. In these studies, the differential equations for the NO concentration inside the fuel particles are solved by numerical methods and because of computational reasons it is not attractive to incorporate the models as sub-models into CFD codes. Yue et al. [42] managed from the governing equations of oxygen, CO and NO inside the char particle to derive an analytical solution for the fractional conversion of char-N to NO. With their model, they successfully predicted the fractional conversion of char-N to NO from oxidation experiments of single coal char particles in a

laboratory scale fluidized bed. Since the model is analytical it is possible to incorporate the model as a sub-model into a CFD code.

For biomass particles few studies report on the reduction of NO inside char particles at combustion conditions. Zevenhoven and Hupa [44] showed that chars from biomass were less reactive with respect to NO than chars from lignite and peat, but more reactive than bituminous coal chars in the temperature range 1023-1223 K. On the other hand, Sørensen et al. [51] showed that chars from raw and washed wheat straw were more reactive with respect to NO than typical coal chars in the temperature range 873-1173 K. Moreover, they determined the apparent reaction order for the NO reduction rate with respect to NO of these two straw chars to be around 0.7. Wang et al. [52] determined the apparent reaction order for NO reduction of straw char to be 0.89 in the temperature range 873-1273 K, while Garijo et al. [53] determined apparent reaction orders to 0.45 and 0.3 for the NO reduction of char from straw and of char from eucalyptus at 1023–1173 K. Dong et al. [54] determined apparent reaction orders for the NO reduction in the temperature range 973-1173 K to be around 0.7 for three biomass chars. The activation energies for the NO reduction reactions in these studies vary between 30 and 110 kJ/mol. Guerrero et al. [55] showed that Eucalyptus chars were more active with respect to NO if prepared with a higher heating rate. On the other hand, Wang et al. [52] showed that a straw char prepared at 1073 K was more active for NO reduction, than the same char prepared at 1273 K. The char prepared at 1273 K was, however, more reactive than the char prepared at 873 K. As for coal chars, the initially formed NO can be reduced inside biomass char particles. Few studies are available on the fractional conversion of char-N to NO during combustion of biomass. Saastamoinen et al. [56,57] modeled the NO formation and reduction inside an entire bed of biomass char particles under grate fired conditions. They used a NO reduction model based on the concentration gradients of NO inside the entire bed of particles.

In this thesis (**Paper IV)** the fractional conversion of char-N to NO is modeled during the oxidation of single char particles of spruce bark. A numerical model based on the governing equations of NO is developed and the analytical model by Yue et al. [42] is tested. Modeled NO release rates, i.e., initial formation minus reduction, are compared to experimental NO release rates from a single particle reactor (SPR) of quartz glass operating at 3-19 vol.% O_2 and at 1073-

1323 K. Moreover, a simplified model based on apparent kinetics is developed (**Paper V**) for predicting the NO release during oxidation of single char particles. Contrary to the numerical NO release models based on the intra-particle NO concentration profiles the apparent kinetics model is simplified to such an extent that it can be incorporated as a sub-model into a CFD code. By using the simplified model, modeled rates of four different biomass chars are compared to experimental measurements from the SPR.

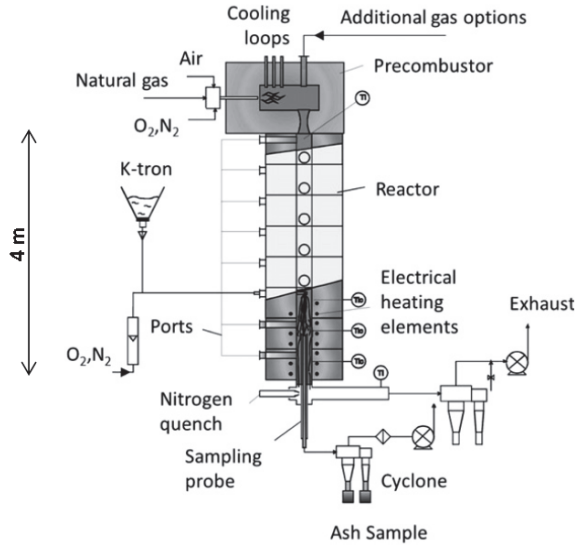

Fig. 12. International Flame Research Foundation (IFRF) isothermal plug flow reactor (IPFR).

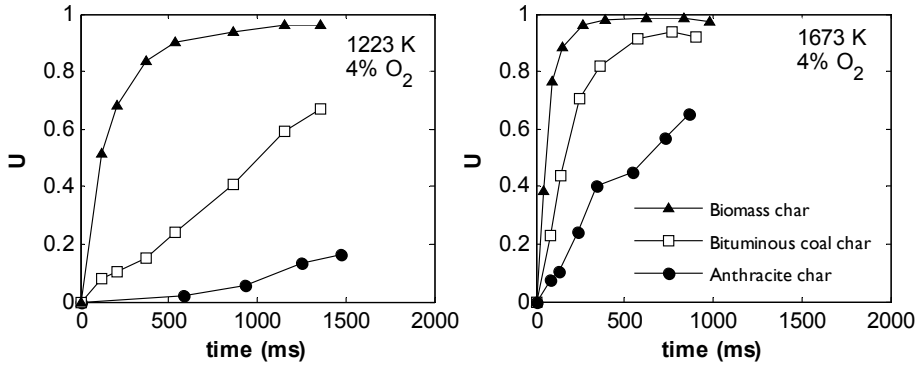

Fig. 13. Raw data for burnout profiles of an anthracite char, a bituminous coal char, and a biomass char obtained from a isothermal plug flow reactor (IPFR) with 4 vol.% O_2 at 1223 K and at 1673 K.

3. Experiments

The experimental data for the char-C oxidation were obtained from an isothermal plug flow reactor described in Chapter 3.1 and the experimental data for the char-N oxidation were obtained from a single particle reactor described in Chapter 3.2.

3.1 Char-C oxidation – Isothermal plug flow reactor

The experimental data on pulverized char-C oxidation were taken from the International Flame Research Foundation (IFRF) solid fuel data base. Prior to the publications of this thesis (Paper I – Paper III), this data has not been published in the literature.

The char oxidation experiments have been performed in an electrically heated 4 m-length vertical isothermal plug flow reactor (IPFR). The reactor is illustrated in Fig. 12. The char samples were prepared in the IPFR at 1473 or 1673 K with around 0.5% oxygen in the surrounding gas. In the char preparation tests the parent coal and biomass particles were fed from the top of the reactor by a vertical probe and the samples were collected at the bottom of the reactor system. Devolatilization times were obtained from the char preparation runs. Based on these times, and typical devolatilization kinetics, the heating rates were estimated to be in the range of 10^4 to 10^5 K/s. In the char oxidation tests, the chars were fed through different horizontal ports situated along the height, and the samples were quenched at the bottom of the system. For each char, the particle burnout fractions at different residence times were obtained using an ash tracer method: the measured ash contents were related to the initial ash contents of the original chars.

The IPFR differs from many drop tube furnaces in such way that the superficial gas velocity is relatively high: 3.5-6 m/s. The inner diameter of the combustion chamber is 150 mm, giving a Reynolds number of around 3000. An advantage with the large diameter is that a higher Reynolds number can be achieved with a lower superficial gas velocity, which is necessary in order to obtain sufficient residence times. Further, the fuel feeding rates were set to achieve a maximum relative decrease in oxygen concentration of 10% over the reactor length. The fuel flow rate was generally around 0.1 kg/h, and the preheated gas flow varied between 40-80 Nm^3/h. The reactor were operated in such way that the temperature distribution in the radial direction and along the

centerline was minimized in order to keep the gas in the reactor as isothermal as possible. This was achieved by a higher Reynolds number compared to conventional drop tube furnaces, the low fuel rates, and the high gas flow rates.

The chars and the experimental conditions investigated are listed in Table 1. In the table, 22 bituminous coal chars, 5 anthracite chars, and 1 biomass char are presented. In general the oxidation tests were performed in the temperature range 1123-1673 K and at 1-3 different oxygen concentrations. For 10 of the 22 bituminous coal chars, oxidation tests were performed using three oxygen concentrations at 1223 K. Only these chars and conditions are considered for the reaction order analysis of the bituminous coal chars. The experimental conditions selected for these 10 chars are marked by using bold font in Table 1.

In the oxidation tests, small quantities of CO_2 and H_2O, resulting from the natural gas burner, were also available in the surrounding gas. Since the particles are so small that the char oxidation by oxygen is far from limited by external diffusion (discussed in chapter 5), and the kinetics of the char oxidation reactions by oxygen are significantly higher than by CO_2 and H_2O at the investigated temperatures, the char consumption by CO_2 and H_2O is not considered in this thesis.

Fig. 13 shows examples of experimental data from the IPFR. The figure shows experimentally determined char oxidation profiles of one bituminous coal char, one anthracite char, and the biomass char. The initial mass mean diameter of the three chars are similar: 42 μm, 39 μm, and 41 μm. The figure shows char oxidation profiles at 1223 K and at 1673 K with 4 vol.% O_2. At both temperatures the char conversion is fastest for the biomass char and slowest for the anthracite char. In the figure it can be seen that the maximum residence time is around 1500 ms. The shortest residence time for which partially burned char particles were collected is around 30 ms.

Table 1.
Parent fuels, experimental conditions

	Fuel	FC%[a]	A%[b]	d (μm)[c]	Exp. Conditions[d]
1.	Columbian coal	59	11	44	[f]**1223/4,8,12 1473/4** 1673/4
2.	Dawmill fine	61	19	40	1223/5 1473/5 1673/5
3.	Douglas prem. (a.f.)[e]	69	12	40	1223/4,8,12 1473/4 1673/4,8,12
4.	Douglas prem. (a.f.)	69	12	36	1223/4,8,12 1473/4 1673/4,8,12
5.	Economy	70	16	61	**1223/4**,6,**8,12** 1373/8 **1473/6** 1573/41673/3
6.	El Cerrejon	61	6	39	1123/5 1473/5 1673/5
7.	Enel coal 2001	59	11	35	**1223/4,8,12 1473/4** 1673/4
8.	Fettnuss	71	4	71	1223/11.9 1473/6 1673/3.4
9.	Genesee	63	28	64	1223/12 1373/8 1473/6 1573/5 1673/3
10.	Gottelborn	63	10	39	1123/5 1473/5 1673/5
11.	Gottelborn < 150	62	9	67	1223/5 1473/5 1673/3
12.	Kellingley 45	67	19	21	**1223/4,8,12 1473/4** 1673/4
13.	Kellingly coarse	62	8	72	**1223/4,8,12 1473/4** 1673/4,8,12
14.	Kleinkopje	72	15	41	1123/5 1473/5 1673/5
15.	Kleinkopje	68	14	19	**1223/4**,6,**8,12 1473/4** 1673/4
16.	Middelburg fine	68	17	42	1223/5 1473/5 1673/5
17.	Polish	66	12	70	1123/5 1473/5 1673/5
18.	Polish	67	4	38	**1223/4,8,12 1473/4** 1673/4
19.	Polish	64	9	24	**1223/4**,6,**8,12 1473/4** 1673/4
20.	Polish 5600	63	15	107	**1223/4,6,8,**12 1373/8 **1473/6** 1573/4 1673/3
21.	South African	63	11	42	**1223/4,8,12 1473/4** 1673/4
22.	Spitsbergen	60	25	57	1223/12 1473/6 1673/3
1.	Anthracite	92	16	35	1223/4,6,8,12 1473/4 1673/4
2.	Charbon Vietnamien	91	30	22	1239/14 1504/9 1683/5
3.	Charbon Chinois	87	16	26	1244/14 1504/9 1673 5
4.	Niederberg	89	10	26	1223/15 1473/10 1673/5
5.	Silo Sample	94	13	39	1223/4,6,8,12 1473/4 1673/4
1.	Beach tree	15	0.4	41	1223/4,8,12 1473/4 1673/4

[a]Fixed-carbon content of parent coal (daf)
[b]Ash-content of parent coal (db)
[c]Mean-mass diameter of char particles
[d]Experimental conditions e.g. for Columbian coal char experiments have been performed at the following reactor temperatures and oxygen concentrations in the gas: 1223 K/4% O_2, 1223 K/8% O_2, 1223 K/12% O_2, 1473 K/4% O_2 and 1673 K/4% O_2.
[e]As fired
[f]The experimental conditions selected for the 10 chars investigated for the reaction order analysis of the bituminous coal chars (Paper I) are marked by using bold font

Fig. 14. Åbo Akademi Single Particle Reactor

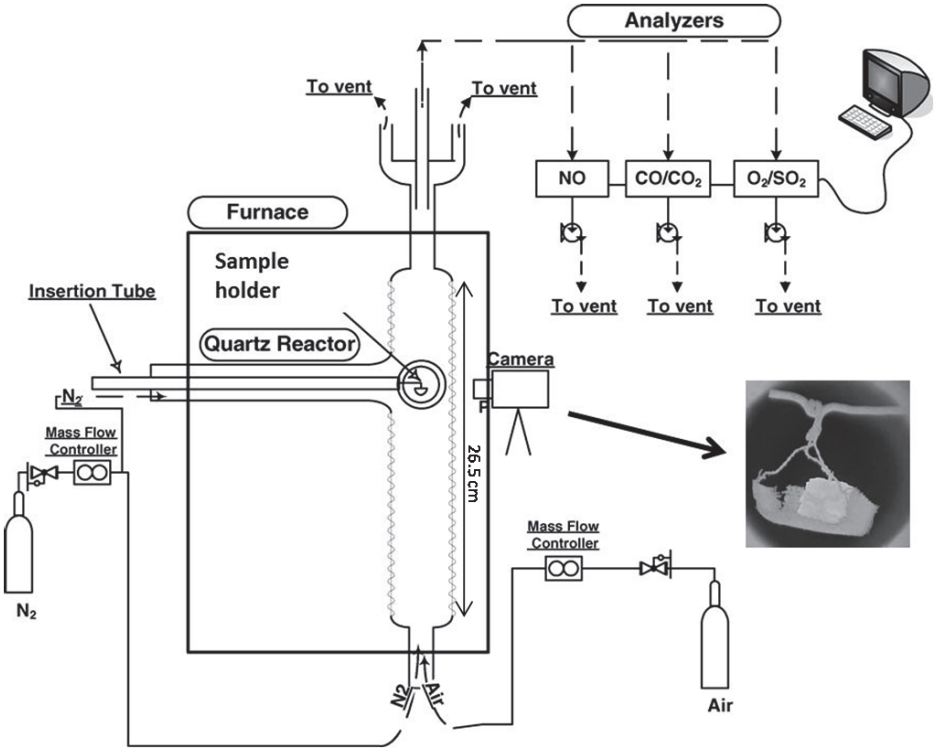

Fig. 15. Single particle reactor and a snap shot of a char particle during the char oxidation stage

3.2 Char-N oxidation – Single particle reactor

NO release from single char particles of biomass were investigated in a single particle reactor of quartz glass at Åbo Akademi University. The investigated biomasses – spruce bark, SRC poplar, straw, and torrefied wood – are listed in Table 2.

Fig. 14 and Fig. 15 show the reactor and a schematic description of the single particle reactor (SPR). The experimental setup consists of a quartz tube reactor inserted in a ceramic furnace. Gas mixtures of synthetic air and nitrogen were fed from the bottom of the reactor system. The temperature of the ceramic walls was electrically heated to the set point temperature and the temperature of the reactor was measured with a thermocouple inserted in the ceramic wall of the furnace. The sample was inserted using a movable probe which could be inserted from a cold environment into the hot reactor within a fraction of seconds. Fig. 15 shows the sample holder which consisted of a thin net, on which the pellets where placed. The net inevitably influenced the temperature of the particle, and the diffusion to and from the particle. However, considering that a small part of the net is in contact with the particle, and the large mesh size, the change in particle temperature and diffusion due to the net was not believed to play a significant role.

Table 2.
Parent biomasses, densities of parent biomasses and chars, elemental analyses.

	FC%[a]	Ash%[a]	C[a]	N[a]	ρ[b]	C[c]	N_{char}[c]	ρ_{char}[d]	K[e]	Na[e]	Ca[e]	Mg[e]
spruce bark	21	4.5	51.2	0.38	1004	75.8	0.39	248	1830	358	8880	794
SRC (poplar)	16	1.7	49.3	0.39	742	83.3	0.59	101	2770	48	4180	421
straw	16	5.5	46.4	0.55	741	70.7	0.61	107	8000	102	3730	711
torrefied wood	27	0.5	57.3	0.12	800	75.6	0.10	245	540	24	1196	258

[a]Fixed carbon content, ash content, carbon content, and nitrogen content of parent fuel (db)
[b]Density of parent fuel (kg/m^3)
[c]Carbon and Nitrogen content of char
[d]Density of char particle (kg/m^3)
[e]mg/kg d.b. of parent fuels

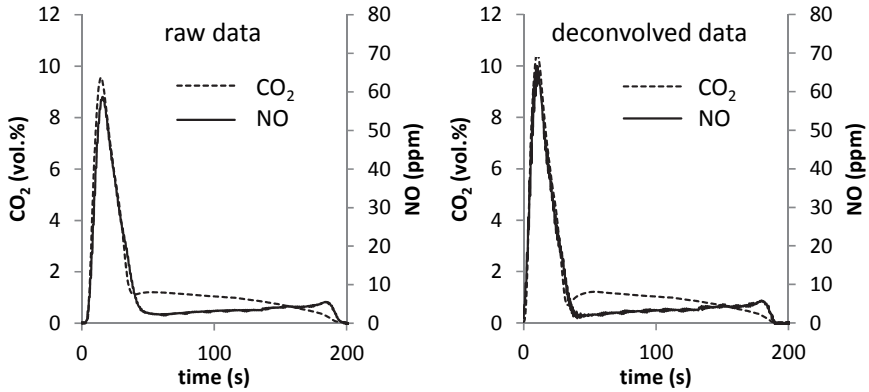

Fig. 16. Measured and deconvolved signal of molar fractions of CO_2 and NO in product gases from biomass particle burning at 1173 K and 19 vol.% O_2

The outlet gas of the reactor system was analyzed using commercial analyzers for the measurement of CO, CO_2, and NO. Fig. 16 shows an example of raw data from the analyzers. The initial peak in the figure corresponds to the devolatilization, and the remaining tail corresponds to the char conversion. In the example, the maximum concentration of CO_2 is around 10 vol.% during the devolatilization, and around 1 vol.% during the char conversion. The maximum concentration of CO for the same condition (not shown here) is around 0.1 vol.% during the devolatilization, and below 0.01 vol.% during the char conversion. Thus, more than 99% of the char-C is oxidized to CO_2 in the reactor system.

The residence time for the gas from the particle to the gas analyzers was around 4 s. Therefore, the measured signal differed from the corresponding signal at the particle. The residence time distribution of the reactor system was taken into account by deconvolving the measured signals. The measured release curves were deconvolved by the derivatives of the residence time distribution for the gas analyzers respectively. Fig. 16 shows measured and deconvolved signals of CO_2 and NO. The local minimum of the deconvolved NO signal, immediately after the peak, is taken as the starting point for the char oxidation. Usually the experiments were repeated three times and the reproducibility was very good: generally the values of the integrals of the experimental NO and CO_2 curves varied less than 2% between the repetitions. The experiments were conducted at 1073, 1173 and 1323 K and with 10 vol.% O_2. At 1173K, experiments were

also performed with 3 and 19 vol.% O_2. The NO and C release rates can be calculated from molar fractions of CO, CO_2 and NO measured at the analyzers:

$$\dot{m}_{C,expt} = \frac{\dot{V}_\infty p}{RT} M_C \left(x_{CO_2}(t) + x_{CO}(t) \right) \quad (1)$$

$$\dot{m}_{NO,expt} = \frac{\dot{V}_\infty p}{RT} M_{NO} \left(x_{NO}(t) \right) \quad (2)$$

Here, $\dot{m}$ is mass stream from the char particle (kg/s); $\dot{V}_{gas}$ is volume flow of gas (m^3/s); p is pressure (Pa); M is molar mass (kg/mol), R is the universal gas constant (J/molK); T is temperature (K); and x is molar fraction.

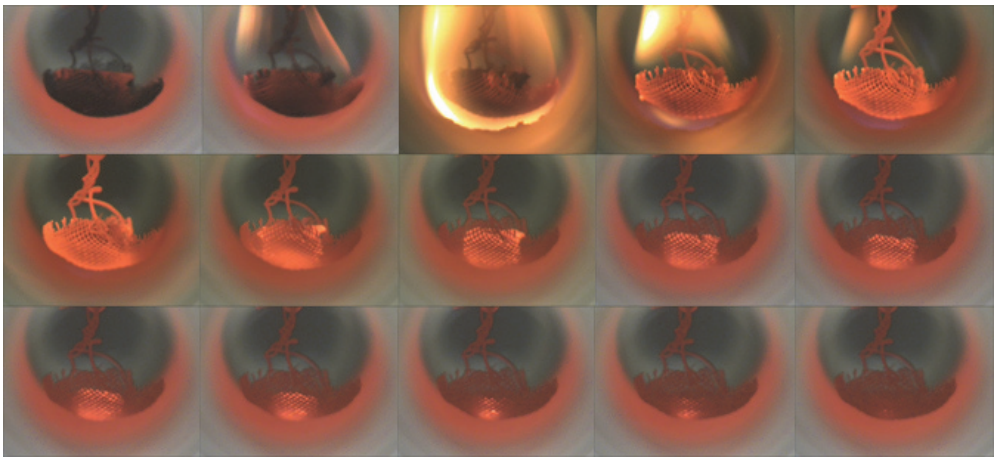

Fig. 17. Snapshots from devolatilization and char oxidation of a single biomass particle. Snapshots 1-5 are during drying and devolatilization, and 6-15 are during char oxidation

The oxidation experiments were recorded with a digital camera. Fig. 17 shows snapshots from a digital video of a torrefied wood pellet during devolatilization and char oxidation. Both during the devolatilization and during the char oxidation, the diameter and the height of the cylinders were measured from the video. The height increased usually by around 100%[1] and the diameter increased by around 10-20% during devolatilization. As the char conversion started, the diameter

[1] In Paper 5 a printing error appeared regarding this number

and height started to decrease, as a result of char consumption close to the surface of the particle. The optical access to the reactor revealed that a stable ash layer was created on the surface of the particle during the char oxidation stage. In the figure, a flame can be seen around the particle. The disappearance of the flame occurred normally within a few seconds before the starting point of the char oxidation as described above.

.

4. Models and determination of parameters

4.1 Char-C oxidation

4.1.1 Char-C oxidation – apparent kinetics model

The model used to predict the char oxidation rates of the pulverized chars is based on apparent kinetics [11,14]:

$$\frac{dm_c}{dt} = S_p k p_{O_2,s}{}^n \qquad (3)$$

Here, m_c is mass of char-C (kg); $p_{O_2,s}$ is the partial pressure of oxygen at the external surface of the particle [2](Pa); and k is the apparent kinetic rate constant

$$k = A_a e^{-E_a / RT_p} \qquad (4)$$

where A_a is the apparent pre-exponential factor (kg/m^{2}sPa^n); E_a is the apparent activation energy; and T_p is the particle temperature. The char consumption rate is also obtained from the incoming flow of oxygen:

$$\frac{dm_c}{dt} = S_p D\left(p_{O_2,\infty} - p_{O_2,s}\right) \qquad (5)$$

Here, D is the external diffusion rate coefficient (kg/m^{2}sPa) and ∞ refers to the bulk phase. Manipulation of Eq. 3 and Eq. 5 to eliminate $p_{O_2,s}$ gives the relationship:

$$\frac{dm_c}{dt} = S_p k\left(p_{O_2,\infty} - \frac{dm_c}{dt}\frac{1}{S_p D}\right)^n \qquad (6)$$

[2] In this thesis both pressure and concentration of oxygen are used following the original publications of this thesis

If n equals to 0, 0.5, or 1, analytical solutions can be derived for the char-C consumption rate. For other reaction orders, the char-C consumption rate must be solved iteratively. The external diffusion rate coefficient D is calculated as:

$$D = G\frac{\left[\left(T_p + T_\infty\right)/2\right]^{0.75}}{d_p} \qquad (7)$$

Here G is a diffusion constant[3] (kg/msPaK$^{0.75}$) [14] and d_p is the diameter of the particle. The temperature of the char particle, T_p, is calculated from the heat balance:

$$m_c c_p \frac{dT_p}{dt} = hS_p\left(T_\infty - T_p\right) - f_h \frac{dm_c}{dt}H + S_p\varepsilon_p\sigma\left(T_{rad}{}^4 - T_p{}^4\right) \qquad (8)$$

where c_p is the heat capacity of the particle (J/kgK); h is the convective heat transfer coefficient (Nuk_∞/d_p); f_h is the fraction of the heat that the particle absorbs from the heat released by the surface reaction H (J/kg); ε_p is the particle surface emissivity; σ is the Stefan-Boltzmann constant; and T_{rad} is the radiation temperature (K). The particles are treated as spherical and the diameter evolution is modeled according to

$$d_p = d_{p,0}\left(1 - U\right)^\alpha \qquad (9)$$

Here *0* refers to initial time; α is the burning mode; and U is the fractional degree of char conversion. In the char oxidation experiments in the IPFR there is a distribution of particle sizes. In this thesis, mono-sized particles are assumed. The mean mass size of the char particles is used as the initial char particle size. By assuming the particles to be mono-sized, it is not possible to model late conversion stages [16,17]. It has been shown that char oxidation models based on apparent kinetics can, however, accurately predict char conversion rates to around 70% of burnout [16,17] when assuming char particles to be mono-sized. Since the size distribution data

[3] In Paper I this unit is incorrect

was generally not available for the pulverized chars in this thesis, only early and intermediate conversion stages were considered, i.e., $U < 0.75$. The following points are presented for clarification:

(i) The Stefen flow is not taken into account, since it is not believed to play an important role for the investigated particle sizes, temperatures, oxygen concentrations and reactivities [58].

(ii) The single reaction product from the char oxidation is assumed to be CO even though there should be some CO_2 formation at the investigated temperatures [10,59].

(iii) Secondary reactions in the boundary layer are not taken into account following Mitchell et al. [60].

(iv) The following values are used: $c_p = 2300$ J/kgK, $f_h = 1$ [14], $\varepsilon_p = 0.85$ [13].

(v) The particles are assumed to follow the gas flow. Thus, the slip velocity between the gas and the particles is assumed to be zero justifying a Nusselt number (*Nu*) of 2.

(vi) The temperatures of the bulk gas and of the furnace walls are assumed to be constant in the model. This is supported by temperature measurements in the reactor.

4.1.2 Determination of parameters

The kinetic parameters for the char-C oxidation have been determined following Murphy and Shaddix [18]. In the determination of the parameters the following least squares-based objective function is minimized:

$$f_{min} = \left(\frac{1}{j_{max} k_{max}} \sum_k \sum_j f_{j,k}^2 \right)^{1/2} \qquad (10)$$

where

$$f_{j,k} = \left(U_{mod} - U_{expt} \right)_{j,k} \qquad (11)$$

Here, the subscript *mod* stands for modeled and *expt* for measured; *j*, *k* refers to the *j*th sampled point in the experiments for the *k*th experimental test condition. In the optimization, A_a is constrained to be positive using the transformation $A_a = e^h$ where *h* is between -25 and +5. The apparent activation energy E_a is constrained to be between 10 and 200 kJ/mol. It may be argued based on the fundamentals that the real activation energy characterizing char oxidation is independent of the reaction order. In the empirical model used in this study, all elementary char oxidation steps are lumped into one step, so it is acceptable that the apparent activation energy is dependent on the apparent reaction order. Thus, the joint optimization of *h* and E_a is conducted separately for each char for various *n*. Note that in ranges of the parameter pairs *h* and E_a which give poor fits between the modeled and the experimental data, the objective functions yield in similar values and as a result the optimization problem is non-convex. In this thesis, *h* and E_a are optimized using a brute force method.

4.2 Char-N oxidation

4.2.1 Char-N oxidation – numerical model

In the NO release models, the char-N is initially assumed to be oxidized to NO. The NO release from the particle is modeled as

$$\dot{m}_{NO} = \dot{m}_{NO,f} - \dot{m}_{NO,r} = z\dot{m}_{NO,f} \qquad (12)$$

where $\dot{m}_{NO,f}$ is the initial formation rate of NO, $\dot{m}_{NO,r}$ is the reduction rate of NO, and *z* denotes the fractional conversion of char-N to NO. The formation rate of NO is calculated here as

$$\dot{m}_{NO,f} = \frac{M_{NO}}{M_N}\frac{Y_N}{Y_C}\dot{m}_{C,expt} \qquad (13)$$

where Y_N and Y_C are fractions of nitrogen and carbon on mass basis in the char and $\dot{m}_{C,expt}$ is the experimental carbon release rate according to Eq. 1. Thus, the char-N is oxidized at the same rate proportionally to the char-C. The initial formation rate of NO, $\dot{m}_{NO,f}$, is directly taken from the experiments in order to minimize uncertainties in the modeling of $\dot{m}_{NO}$ in Eq. 12. The NO reduction reactions can be simplified with the following mechanism:

$$NO(g) + CO(g) \rightarrow \tfrac{1}{2} N_2(g) + CO_2(g) \qquad (R1)$$

$$NO(g) + C(s) \rightarrow \tfrac{1}{2} N_2(g) + CO(g) \qquad (R2)$$

The relative importance of R1 and R2 varies with the temperature and is not well understood [32,44]. In this study, the NO reduction rates are lumped together, therefore, and expressed as $k_{NO}C_{NO}^{\gamma}$ where $k_{NO} = A_{i,NO}e^{-E_{i,NO}/RT_p}$ is the kinetic rate constant and C_{NO} is the concentration of NO (mol/m^3). Here, $A_{i,NO}$ is the pre-exponential factor ((mol/m^3)$^{1-\gamma}$/s); $E_{i,NO}$ is the activation energy (kJ/mol); and γ is the reaction order for the NO reduction. Lu et. al [61] showed that temperature gradients exists in large char particles oxidized at high temperatures. For simplification, however, the char particles are assumed to be isothermal in a given time step. The particle temperature is calculated from Eq. 8. To calculate the particle temperature, ε_p is assumed to be 0.6 following Chen and Kojima [62]. In the oxidation of the char, both CO and CO_2 are formed as reaction products. According to preliminary camera pyrometer measurements in the SPR, the char particle surface temperature is close to the temperature obtained from the assumption that CO_2 is the sole reaction product. Therefore, *H* is calculated by assuming that that the reaction product is CO_2.

The parent fuel particle is cylindrical, but after devolatilization, i.e., as the char oxidation starts, the particle shape has been changed and corresponds to something between a cylinder with an aspect ratio of around one and a sphere. Here, S_p is calculated from the external surface area of a spherical particle. The initial value of the external char particle diameter is taken from the video, and the development of d_c is modeled assuming the particle to be shrinking with a constant

density. Thus, d_c is initially equal to d_p, but as the conversion proceeds, an ash layer is formed around the particle and d_c is smaller, therefore, than d_p.

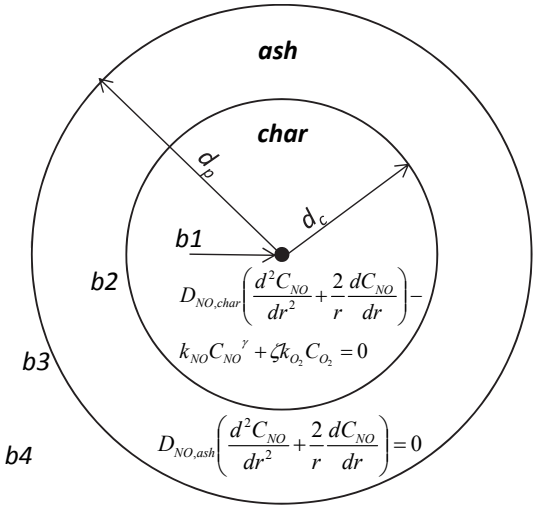

Fig. 18. Intrinsic NO release model

The equations for the concentration of NO inside and outside the particle are illustrated in Fig. 18. Inside the particle, the governing equation for NO is

$$D_{NO,c}\left(\frac{d^2C_{NO}}{dr^2}+\frac{2}{r}\frac{dC_{NO}}{dr}\right)-k_{NO}C_{NO}{}^{\gamma}+\zeta k_{O_2}C_{O_2}=0 \qquad (14)$$

The O_2 concentration in the char particle is calculated from

$$D_{O_2,c}\left(\frac{d^2C_{O_2}}{dr^2}+\frac{2}{r}\frac{dC_{O_2}}{dr}\right)-k_{O_2}C_{O_2}=0 \qquad (15)$$

Here $D_{NO,c}$ and $D_{O_2,c}$ are diffusion coefficients of NO and O_2 in N_2 as determined for wood char: $D_{i,c}=0.20\,D_{i,\infty}$ [63]. The concentrations outside the particle are obtained from:

$$D_i\left(\frac{d^2C_i}{dr^2}+\frac{2}{r}\frac{dC_i}{dr}\right)=0 \qquad (16)$$

In any time step, Eq. 14 and Eq. 15 are solved inside the char core of the particle. Eq. 16 is solved in the ash layer of the particle and outside the ash layer of the particle. Eq. 14 and Eq. 15 are solved using the boundary conditions at the center of the particle:

$$\frac{dC_i}{dr}=0 \qquad (17)$$

and at the surface of the char core:

$$C_i=C_{i,c} \qquad (18)$$

At the outer layer of the char core, C_{O_2} is solved by iteration in such a way that the incoming flow of oxygen assuming Fick´s law equals the consumption of oxygen. Correspondingly, C_{NO} is solved in such way that the produced NO equals the NO that diffuses away from the particle. As pointed out previously the initial NO formation rate is calculated from the experimental char-C oxidation rate. The char-C oxidation rate is, however, also modeled, but only in order to get the position inside the particle for the initial NO formation. Inside the ash layer, Eq. 16 is solved using the boundary conditions in Eq.18 and at the external surface of the ash layer from:

$$D_i\frac{dC_i}{dr}=K_i\left(C_{i,\infty}-C_i\right) \qquad (19)$$

where K_i is the external mass transfer coefficient. Because the ash porosity is very high, the diffusion coefficient in the ash layer is assumed to be the same as in the gas phase. The external mass transfer coefficient is calculated from:

$$K_i = \frac{ShD_i}{d_p} \tag{20}$$

where

$$Sh = 2 + 0.6 Re^{0.5} Sc^{1/3} \tag{21}$$

$$Re = \frac{ud_c}{v} \tag{22}$$

$$Sc = \frac{\nu}{D} \tag{23}$$

Here *Sh, Re,* and *Sc* are the Sherwood number, the Reynolds number, and the Schmidt number respectively. In the equations, *u* is the slip velocity (m/s) between the surrounding gas and the particle; and *v* is the kinematic viscosity (m^2/s). In the bulk phase the boundary conditions for Eq. 16 are the ones in Eq. 19 and:

$$C_i = C_{i,\infty} \tag{24}$$

The bulk phase NO concentration is calculated from the NO release from the particle divided by the total molar flow of the reactor systems. The differential equations described in this section are solved by the difference method by discretizing both the particle and the region outside the particle into 50 layers. When the number of layers is further increased, the results are not changed notably.

4.2.2 Char-N oxidation – analytical model

The analytical model by Yue et al. [42] has been successfully used under laboratory-scale fluidized bed conditions. In this thesis the analytical model is tested for a single char particle

oxidized in a stream of gas. In the model, first order kinetics is assumed for the NO reduction inside the char particle. The concentration of NO is obtained from

$$D_{NO,c}\left(\frac{d^2C_{NO}}{dr^2}+\frac{2}{r}\frac{dC_{NO}}{dr}\right)-\left(k_{CO}C_{CO}+k_{NO}\right)C_{NO}+\zeta k_{O_2}C_{O_2}=0 \qquad (25)$$

To solve this equations analytically, the boundary condition at the surface of the particle ($r = R$) is

$$C_{NO}=0 \qquad (26)$$

and in the center of the particle:

$$\frac{dC_{NO}}{dr}=0 \qquad (27)$$

The boundary conditions in Eq. 26 and Eq. 27 are simplifications required to obtain analytical solutions. If the particle were surrounded by a very thin boundary layer, the NO concentration would rapidly decrease outside the particle. In such a case, the boundary conditions in Eq. 26 can be justified. Based on analytical solutions of the concentrations of O_2 and NO inside the particle [42], the fractional conversion of char-N to NO can be calculated from

$$z=\frac{Th_{O_2}^2}{Th_{O_2}^2-Th_{NO}^2}\frac{Th_{O_2}\cosh\left(Th_{O_2}\right)-Th_{NO}\sinh\left(Th_{O_2}\right)\coth\left(Th_{O_2}\right)}{Th_{O_2}\cosh\left(Th_{O_2}\right)-\sinh\left(Th_{O_2}\right)} \qquad (28)$$

Here, Th_{O_2} is the Thiele modulus for the char-C oxidation:

$$Th_{O_2}=\frac{d_p}{2}\sqrt{\frac{K_{O_2}}{D_{O_2,c}}} \qquad (29)$$

and Th_{NO} is the Thiele modulus for the NO reduction (R1 and R2):

$$Th_{NO} = \frac{d_p}{2}\sqrt{\frac{K_{CO}C_{CO,c} + K_{NO}}{D_{NO,c}}} \qquad (30)$$

Since $C_{CO,s}$ is zero in the analytical model, $K_{CO}C_{CO,s} + K_{NO}$ is equal to K_{NO} and correspondingly the Thiele modulus for NO required in Eq. 28 becomes

$$Th_{NO} = \frac{d_p}{2}\sqrt{\frac{K_{NO}}{D_{NO,c}}} \qquad (31)$$

4.2.3 Char-N oxidation – apparent kinetics model

In this section a simplified NO release model is presented. The NO release is expressed in the same way as Eq. 12:

(NO release) = (initial formation of NO) – (reduction of NO inside char particle) (32)

In the simplified model the initial formation of NO is assumed to be proportional to the char-C consumption rate as in Eq. 13. As a consequence the first term on the right hand side in Eq. 32 is dependent on the particle size similarly as the char-C oxidation rate depends on the particle size. For the biomass char particles considered in this study, the char-C oxidation rate can be assumed to be limited by external mass transfer of oxygen. Under such Regime III conditions, the concentration of oxygen approaches zero at the external surface of the particle, and outside the boundary layer of the particle the oxygen concentration equals the bulk concentration of oxygen. Note that that the boundary layer is undefined in a stagnant surrounding. By disregarding homogenous reactions by oxygen, the concentration profile of oxygen outside the particle is obtained from Eq. 16. With the boundary conditions at $r_p : C_{O_2} = 0$ and at $r_p + \delta : C_{O_2} = C_{O_2,\infty}$, where δ is the thickness of the boundary layer of the particle, Eq. 16 can be solved to give the oxygen flux to the surface of the particle:

$$\dot{n}_{O_2} = D_{O_2,\infty} \frac{C_{O_2,\infty}}{\left(\frac{1}{r_p} - \frac{1}{r_p + \delta} \right)} \qquad (33)$$

For $\delta \to \infty$, Eq. 33 is simplified to $\dot{n}_{O_2} = r_p D_{O_2,\infty} C_{O_2,\infty}$ and the oxygen flux is thus proportional to the radius of the char particle. For $\delta \to 0$, the oxygen flux approaches infinity. By assuming that δ otherwise is roughly proportional to the radius of the char core, Eq. 33 can be manipulated in such way that the oxygen flus is proportional to the radius. Thus, the first term on the right hand side in Eq. 32 can be assumed to be approximately proportional to the radius of the particle. Concerning the second term on the right hand side in Eq. 32, it has been shown that the relative NO reduction increases as a function of increasing particle size [41-43]. Based on this, the second term must be more strongly dependent on the particle size than the first term, and the NO reduction can be assumed to be proportional to the external surface area of the char particle. With these assumptions, Eq. 32 can be expressed as

$$\dot{m}_{NO} = \frac{M_{NO}}{M_N} \frac{Y_N}{Y_C} \dot{m}_{C,expt} - p^n_{NO,\max} S_p A_{a,NO} e^{-E_{a,NO}/RT_p} \qquad (34)$$

Here $A_{a,NO}$ is the apparent pre-exponential factor (kg/m^{2}sPa^n); $E_{a,NO}$ is the apparent activation energy (J/mol); and n is the apparent reaction order for the NO reduction inside the char particle. The particle temperature is calculated in the same way as with the numerical model. The approximated theoretical maximum of the partial pressure of NO, $p_{NO,\max}$, is defined as

$$p_{NO,\max} = \frac{x_N}{x_C} p_{O_2,\infty} \qquad (35)$$

At the temperatures considered in this study, the combustion of the large particles is expected to be controlled by external diffusion, except for the very late conversion stages and, therefore, the partial pressure of oxygen is near zero at the external surface of the particle. The binary diffusion coefficients of CO and CO_2 differ slightly from the binary diffusion coefficient of O_2 in N_2, but

the maximum partial pressure of CO and CO_2 will be close to the partial pressure of O_2 in the bulk gas [3]. By also considering that the differences in the binary diffusion coefficients of CO or CO_2 in N_2 and NO in N_2 are small and that the oxidation of carbon and nitrogen is non-selective, the partial pressure of NO can be related to the partial pressure of O_2 as in Eq. 35.

4.2.4 Determination of parameters

The kinetic parameters for the NO release models have been determined by minimizing the objective function

$$f_{min} = \sqrt{\frac{1}{j_{max}} \sum_{j} f_{min,j}^{2}} \qquad (36)$$

where

$$f_{min,\,j} = \left(\sum_{t=0} \dot{m}_{NO,expt}(t) \right)^{-1} \sum_{t=0} \left| \dot{m}_{NO,expt}(t) - \dot{m}_{NO}(t) \right| \qquad (37)$$

Here, t = 0 is the time for when the char combustion begins, and j is number of experiment, i.e., five in this thesis. In the analytical and numerical model A_{i,O_2} and E_{i,O_2} are constrained in such way that Th_{O_2} must be larger than 100 the for the initial char particle radius at 1073K, and γ is fixed at one. With this assumption, the char oxidation is always mass transfer limited (except for the very final degrees of conversion due to very small particle sizes). It is not possible to determine A_{i,O_2} and E_{i,O_2} from the measurements directly, since the conversion is nearly limited by external diffusion of oxygen, i.e., Regime III conditions. Moreover it is important to note that A_{i,O_2} and E_{i,O_2} are not used to model the carbon release rate; the carbon release rate is taken directly from the measurements. However, A_{i,O_2} and E_{i,O_2} are used to get the position in the char particle where the NO is formed, i.e., close to the external surface of the particle. For the simplified model, only three parameters are determined for each fuel char and a brute force method has been used for the determination of the parameters. For the numerical model the parameters have been determined by using a genetic algorithm based on differential evolution.

5. Results

5.1 Char-C oxidation

5.1.1 Reaction orders of bituminous coal chars

Fig. 19 shows minimized objective functions as a function of the reaction order for the 10 bituminous coal chars. The reaction orders giving the best fit are generally close to one, although a distribution of reaction orders can be used to obtain similar values of the objective functions as in the optimum cases. To take one example, Fig. 20 plots modeled and experimental char oxidation profiles for the South African char using n = 0.50, n = 0.79, n = 1.00, and n = 1.08. Note that the kinetic parameters vary for each reaction order. It can be seen that both n = 1.00 and n = 0.79 give reasonable fits between the modeled and experimental burnout profiles to around 70% of burnout. For n = 0.5, the fit can be regarded as inadequate. For the latter case, at 1223 K and 4 vol.% O_2, the model strongly overestimates the char oxidation rate, while at 12 vol.% O_2 the model underestimates the char oxidation rate. The differences between the optimum objective function values for n and n_{opt} are included in the figure: when n = 1.00, the difference is 0.001; when n = 0.79, it is 0.01; and when n = 0.50, it is 0.034.

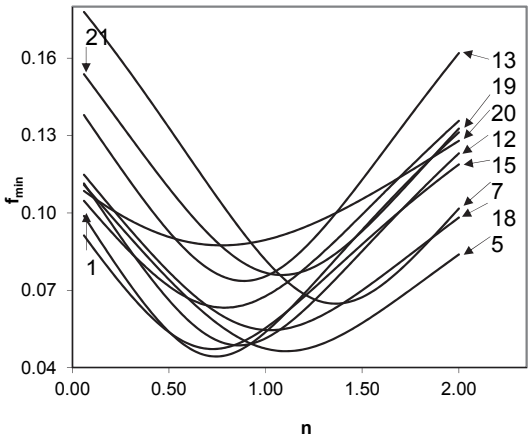

Fig. 19. Minimized objective function versus apparent reaction order for 10 bituminous coal chars.

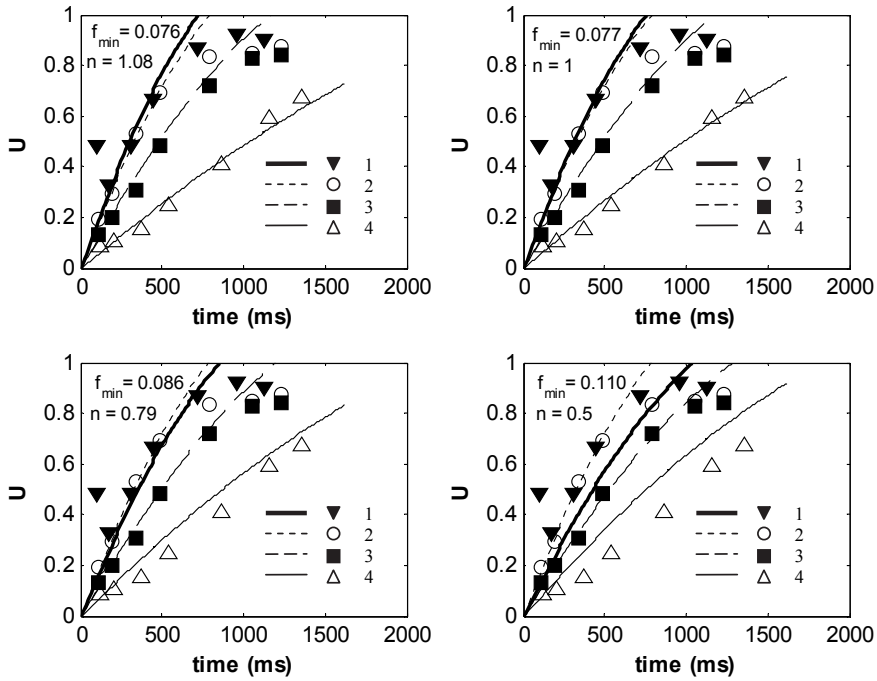

Fig. 20. Modeled and experimental burnout versus residence time with various apparent reaction orders for a South African coal char. The symbols represent the experimental data, and the lines represent the modeled data. Conditions 1–4 refer to (1) 1223 K/12% O_2; (2) 1473 K/4% O_2; (3) 1223 K/8% O_2; and (4) 1223 K/4% O_2.

Fig. 21 shows the minimized objective function as a function of the fixed-carbon content of the parent coal of the chars with $n = 0.5$, $n = 1$, and by using the optimum n. The figure shows the difference between the objective functions for n_{opt} and for (i) $n = 0.5$ and (ii) $n = 1$. There is no obvious relationship between the reaction order and the fixed-carbon content of the bituminous coal chars. Moreover it can be seen that $n = 1$ gives better fits between the modeled and experimental burnout profiles than $n = 0.5$. For $n = 0.5$, the objective function difference is < 0.01 for four of the 10 chars, while $n = 1$ yields differences < 0.01 for nine of the 10 chars. The char for which $n = 1$ gives a fit above 0.01 is the *Enel coal* char; its reaction order is discussed below.

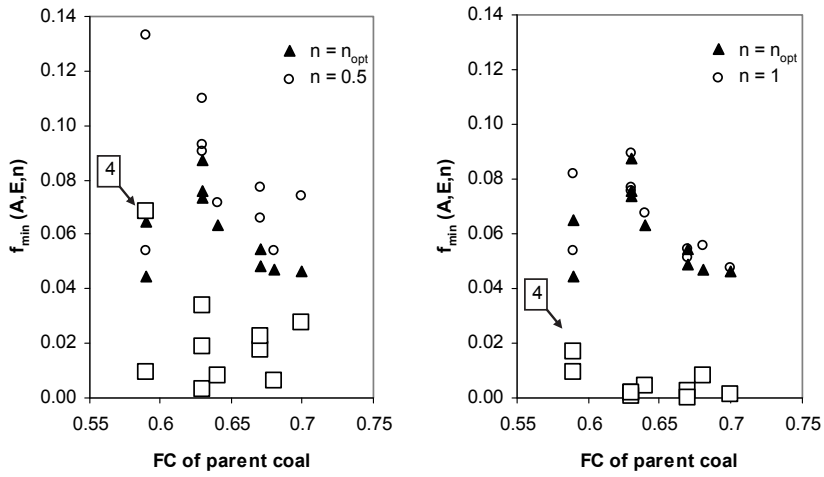

Fig. 21. Minimum values of objective functions using the optimized kinetic parameters and apparent reaction order (filled triangles), and of objective functions with a fixed value for the apparent reaction order and optimized kinetic parameters (circles) for ten bituminous coal chars. Each set of points (one triangle, one circle) represents one char. The squares represent the differences between the minimum values of the objective functions (triangles and circles) for each char.

For the Enel coal char n_{opt} = 1.36, and the minimum value of the objective function is 0.063. For n = 0.5 and n = 1, the minimum values of the objective functions are 0.133 and 0.082, respectively. Fig. 22 shows the modeled and experimental burnout profiles of the char from the Enel coal, using n = 0.5, n = 1, and n = 1.36. The experimental burnout profiles at 4 and 12 vol.% O_2 differ significantly; an increase in the oxygen concentration affects the burning rate strongly, implying a high reaction order. However, a reaction order of 1.36 appears to be unrealistic. In the figure, two outliers which might explain the high apparent reaction order are marked. Repeating the optimization without the outliers gives an optimum reaction order of 1.19. In this case, n = 1 gives an objective function less than 0.01 from the optimum case. Nevertheless, whether the outliers are included or excluded, n = 1 is a better alternative than n = 0.5.

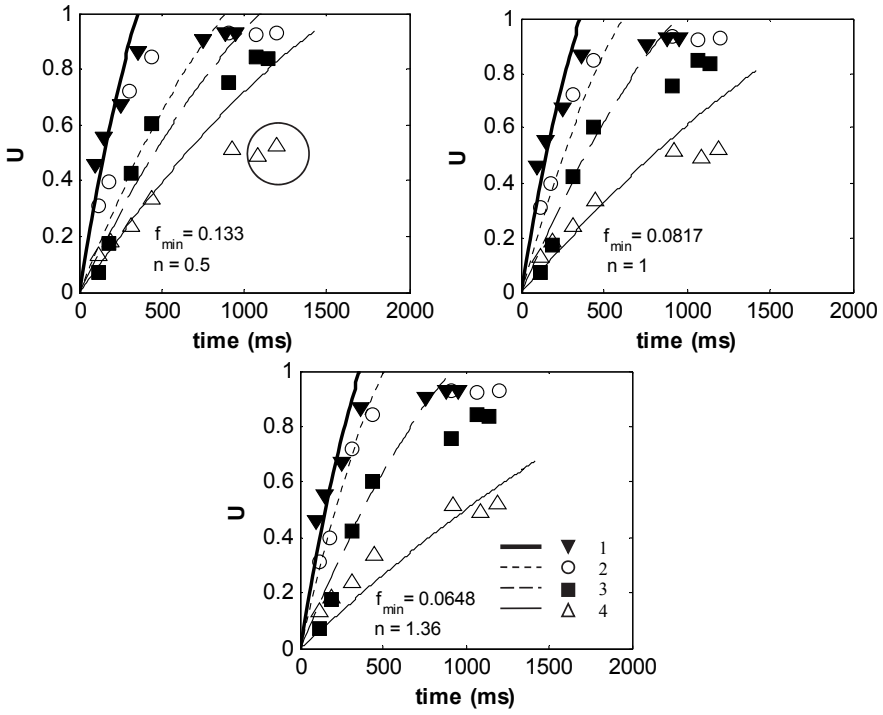

Fig. 22. Modeled and experimental burnout versus residence time with various apparent reaction orders for an Enel coal 2001 char. The symbols represent the experimental data, and the lines represent the modeled data. Conditions 1–4 refer to (1) 1673 K/4% O_2; (2) 1223 K/12% O_2; (3) 1223 K/8% O_2; and (4) 1223 K/4% O_2. The experimental outliers are marked with a circle.

Since the char oxidation is strongly exothermal, the relationship between the apparent reaction order and the activation energy must be considered: an increase in the oxygen concentration gives higher particle temperatures, which give faster burning rates due to faster chemical kinetics. The assumption that the oxidation product is solely CO_2 will lead to overestimation of the particle temperatures during the oxidation of pulverized char particles [14,18]. Fig. 23 plots the mean objective function F of the 10 chars as a function of n:

$$F(n) = \frac{1}{N} \sum_{char=1}^{N} f_{\min}\left(E_a, A_a, n\right) \qquad (38)$$

The optimum apparent reaction orders of the 10 chars based on the mean objective function given by Eq. 38 are 0.93 and 0.82 when the reaction product is CO or CO_2, respectively. Fig. 23 shows that $n = 1$ is a better alternative than $n = 0.5$ for the 10 chars, with either CO or CO_2 as the single reaction product.

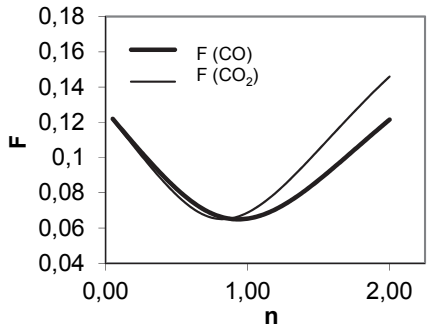

Fig. 23. Mean of the objective functions *F* as a function of the apparent reaction order, for ten bituminous coal chars, with reaction product CO or CO_2.

As pointed out in the introduction of the thesis, several studies have reported reaction orders of one at Regime II conditions for bituminous coal char. Nevertheless, the true reaction order for char-C oxidation has generally been suggested to 0, which under Regime II conditions frequently is assumed to correspond to an apparent reaction order of 0.5. Thus, this is in contrast to the determined reaction orders of this thesis. Conventionally, reaction orders are determined by changing the oxygen concentration of the gas at a given gas temperature. As the oxygen concentration increases, the particle temperature increases, enhancing the kinetic rates of the reactions. Therefore the activation energy needs to be known. However, in order to determine the activation energy under Regime II conditions, the reaction order needs to be known.

To demonstrate this problem, kinetic parameters are determined for the *Economy* char by using an Arrhenius plot. In this procedure the logarithmic rate divided by the surface pressure of oxygen and the external surface area is plotted versus the inverse temperature. Here the rate is taken from the experimental data and the pressure of oxygen at the external surface is calculated by taking the external diffusion into account (see Eq. 3 and Eq. 6).

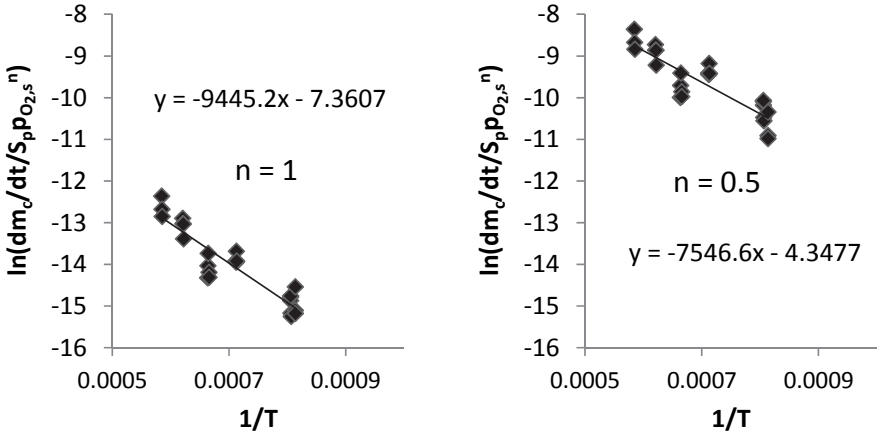

Fig. 24. Logarithmic rate versus inverse temperature by assuming the apparent reaction order to (i) 1 and (ii) to 0.5.

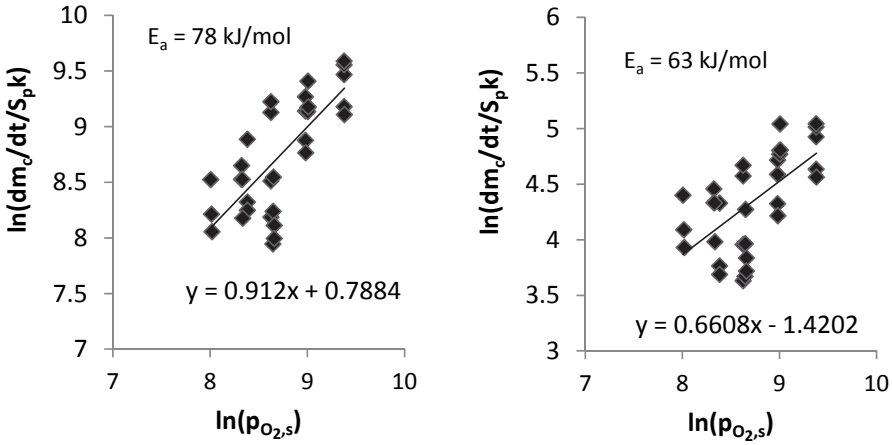

Fig. 25. Logarithmic rate versus logarithmic partial pressure of oxygen at the external surface of the particle by assuming the activation energy to (i) 78 kJ/mol and (ii) to 63 kJ/mol.

Fig. 24 shows such a rate versus the inverse temperature for the *Economy* char using (i) $n = 1$ and (ii) $n = 0.5$. The activation energy is calculated from the slope and is 78kJ/mol in the first case and 63 kJ/mol in the second case. From the multivariable optimization the objective function is 0.114. By using the parameters from the Arrhenius-plot the objective functions are 0.13 and 0.17 with n = 1 and 0.5, respectively. The apparent reaction order can be obtained by plotting the logarithmic rate divided by the kinetic rate constant and external surface area versus the

logarithmic surface pressure of oxygen (see Eq. 3). Fig. 25 shows such plots by assuming the apparent activation energy to (i) 78 kJ/mol and (ii) 63 kJ/mol. In the first case, the optimum reaction order is 0.91 and in the second case the optimum reaction order is 0.66. Thus the reaction order is, as expected, strongly dependent on the value of the activation energy under Regime II conditions. For the experimental data of the Economy char, fixing the activation energy to a low value gives a lower apparent reaction order than fixing the activation energy to a higher value. Conventionally it is assumed that the apparent activation energy under Regime II conditions is half of the activation energy determined under Regime I conditions [11]. This is complicated, however, due to the fact that the rate limiting steps differ as a function of temperature Char-C oxidation can be simplified with the two following lumped reactions:

$$2C(s) + O_2(g) \rightarrow 2CO(g) \qquad (R3)$$

$$C(s) + O_2(g) \rightarrow CO_2(g) \qquad (R4)$$

The activation energy of the first reaction is higher than of the second reaction and, therefore, the CO/CO_2 ratio increases as a function of increasing temperature. Geier et al. [10] showed numerically that this ratio can be around 0.5 at temperatures characterizing Regime I conditions, while the ratio can be around 10 at temperatures characterizing Regime II conditions. Therefore, if the apparent activation energy is determined under Regime I conditions and extrapolated to Regime II conditions (divided by two) the apparent activation energy will be underestimated at Regime II conditions, since the activation energy of the first step is higher than of the second step. Following Fig. 25, this would lead to an underestimation of the apparent reaction order. Thus, to determine kinetic parameters and reaction orders for char-C oxidation under Regime II conditions, the two conventional ways – TGA-tests and Arrhenius-plots – can be questioned.

5.1.2 One-parameter model for bituminous coal chars

By fixing the apparent reaction order to one, apparent activation energies have been determined for the 22 bituminous chars. Fig. 26 shows the apparent activation energies of the 22 chars. The activation energies are plotted as a function of fixed-carbon content of the parent coals. There is no obvious relationship between the activation energies and fixed-carbon contents of the parent

coals. The activation energies lie between 48 and 99 kJ/mol and are listed in Table 3. These values are in agreement with reported values and are typical for Regime II conditions [e.g. 3,4,7,11,17,18,21,22,28-31]. It is, however, useful to compare the char oxidation rates to rates limited by external diffusion. The maximum values of these fractions are generally below 0.05 at 1223 K. At this temperature, the highest value was observed for the Genesee char, i.e., 0.27. Correspondingly, the fractions are generally around 0.10-0.20 at 1673 K. Also at this temperature, the highest value was observed for the Genesee char, i.e., 0.38. Thus, it is likely that the oxidation of the 22 chars occur under Regime II conditions.

Fig. 27 illustrates a contour diagram of A_a and E_a for a Polish coal char; the contours correspond to the values of the objective function in Eq. 10. The optimum E_a is 85 kJ/mol. The figure shows that a range of parameter combinations of A_a and E_a can be used to yield a similar value of the objective function, as in the optimum case.

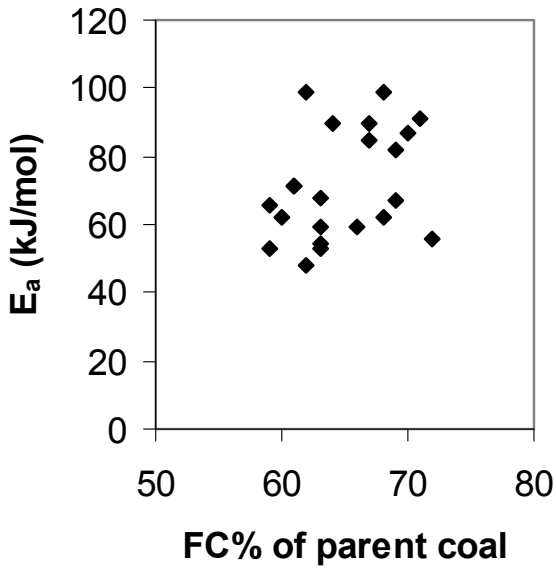

Fig. 26. Apparent activation energies of 22 bituminous coal chars

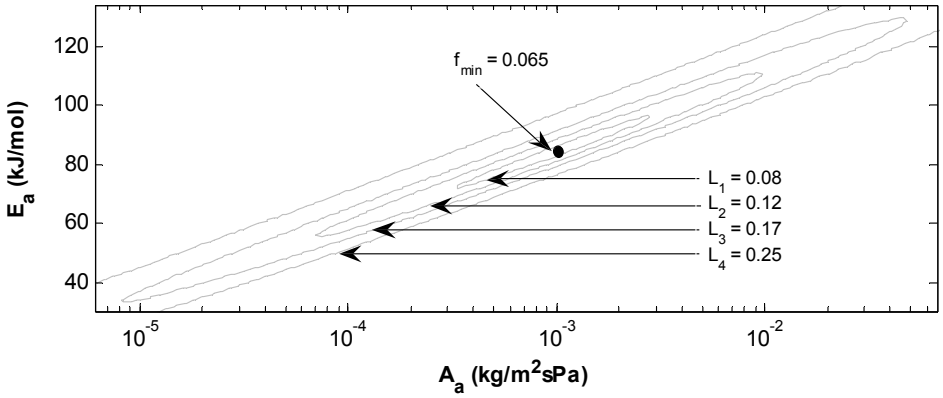

Fig. 27. Contour diagram of the apparent pre-exponential factor and apparent activation energy of a Polish coal. The values indicated on the contours correspond to the values of the objective function. The minimum is marked with a filled circle

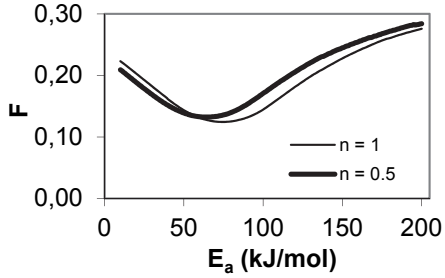

Fig. 28. Mean objective function as a function of the apparent activation energy of 22 bituminous coal chars with apparent reaction order of 0.5 and 1.

Fig. 28 displays the mean objective function (Eq. 38) as a function of the constant apparent activation energy for the 22 chars. The optimum constant apparent activation energy is 74 kJ/mol. In the figure, the mean objective function curve is also displayed for $n = 0.5$. The mean objective function is slightly higher for this case and the value of the constant apparent activation energy decreases to 64 kJ/mol. Fig. 29 illustrates the objective functions for the 22 coal chars when E_a is separately determined for each char, and when $E_a = 74$ kJ/mol for all the chars. Note that the pre-exponential factors are determined separately for each char and activation energy. Generally, the objective functions are similar in both cases, implying that the constant activation energy of 74 kJ/mol is appropriate. To test whether there is any statistical difference in the two groups of objective functions, the following opposing hypothesis is tested: the expected value of the

objective functions with E_a = 74 kJ/mol (population 1) is higher than the expected average value of the objective functions with E_a optimized separately for each char (population 2). Here, the expected average value of population 2 is assumed to be equal to the mean value of population 2, that is, 0.114. To test the hypothesis, a one-sided confidence interval is calculated for population 1:

$$I_\mu = \left(\bar{x} - \frac{t_\alpha(v) s_x}{\sqrt{n}} ; \infty \right)$$

where $\bar{x}$ is the mean value of population 1, 0.126; t_α is the t-quintile; s_x is the standard deviation; n is the size of the population; and $v = n - 1$. The confidence interval equals to I_μ = (0.109; ∞) with a significance level of 0.05. According to the confidence interval, the expected value of population 1 can be smaller than the expected average value of population 2 and, as a consequence, the hypothesis cannot be accepted. Based on this a constant activation energy of 74 kJ/mol can be used for the investigated conditions.

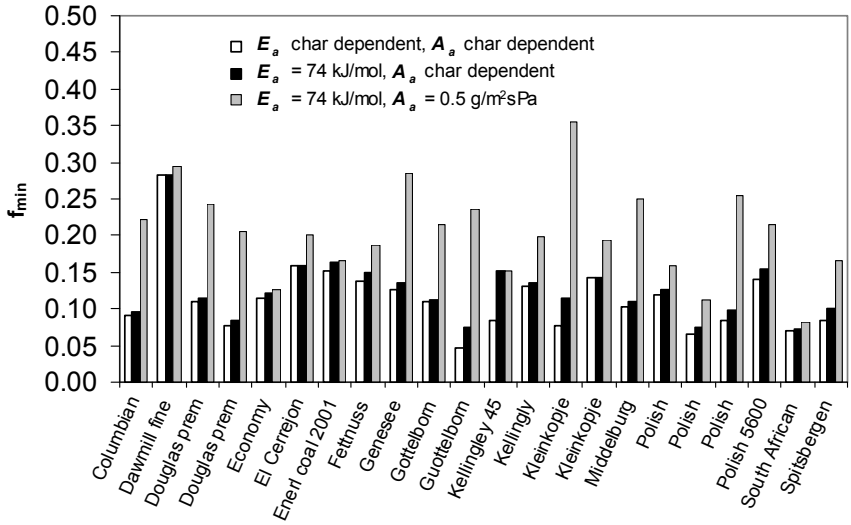

Fig. 29. Minimum values of objective functions using the optimized activation energies for 22 chars, of objective functions using constant a activation energy for the 22 chars, and of objective functions using constant activation energy and constant pre-exponential factor for the 22 chars

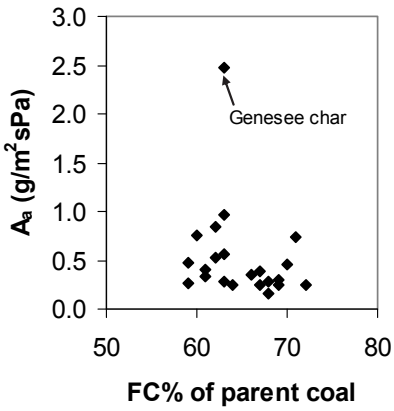

Fig. 30. Apparent pre-exponential factors of 22 bituminous coal chars with a constant apparent activation energy of 74 kJ/mol for each char versus fixed carbon content of the parent coal.

With a constant E_a and n, A_a is the single fuel specific parameter. In such a case the difference in A_a corresponds to the difference in the reactivity. Fig. 30 shows A_a (with constant E_a of 74 kJ/mol) of the 22 chars as a function of the fixed-carbon content of the parent coals. For 21 of the 22 chars A_a vary between 0.2 and 1 g/(sm^2 Pa), while A_a of the Genesee char is 2.5 g/(sm^2 Pa), Thus, the kinetic rate for the Genesee char is more than 12 times higher than the coal chars with the lowest reactivity, i.e., the lowest value of A_a. To demonstrate the influence of A_a on the objective function, the objective functions of the 22 chars have been calculated with A_a = 0.5 g/(s m^2 Pa) for the 22 chars, because most of A_a is in the proximity of 0.5 g/(sm^2 Pa), for the chars. In Fig. 29, the objective functions with all the kinetic parameters fixed for the 22 chars are illustrated, i.e., A_a = 0.5 g/(sm^2 Pa), E_a = 74 kJ/mol, and n = 1. The figure shows that the objective functions, and thus the difference in the fits between modeled and experimental data, increase significantly when A_a is fixed compared to when A_a is char specific. The char reactivity is a function of active surface area available for reaction, distribution of active sites, and catalytic elements. Since the internal surface area is not available for the 22 chars, it is not possible to further correlate the pre-exponential factors with the properties of the coals and the chars.

Fig. 29 and the analyses above show that only one parameter is required to predict char oxidation rates of bituminous coal chars under Regime II conditions. This has not been demonstrated

previously by using apparent kinetic models and it simplifies the use of such a sub-model in CFD codes, since fewer parameters need to be determined.

As pointed out, the model cannot be used for predicting late degrees of char conversion and carbon in ash in CFD modeling of pulverized fuel combustion. More detailed models are required for this. It is also important to point out that the model has been tested for a limited range of conditions. At the highest gas temperatures considered, generally 1673 K, the oxygen concentrations in the gas were generally 4 vol.%. According to the model, the particle temperatures approaches 1800 K and the particle surface concentrations of oxygen is significantly below 4 vol.% O_2 under such conditions. Although the temperature and the oxygen concentration varies as functions of degree of char conversion, particle trajectories, and boiler type, these conditions are not far from the conditions where most of the char is oxidized in pulverized fuel boilers.

Table 3.
Parent coals, kinetic parameters of chars

Coal:	E_a [a]	A_a [a]	A_{74} [a]
Columbian coal	66	0.131	0.264
Dawmill fine	71	0.304	0.410
Douglas prem. (a.f.) [g]	67	0.143	0.254
Douglas prem. (a.f.)	82	0.564	0.298
Economy	87	1.430	0.453
El Cerrejon	71	0.259	0.329
Enel coal 2001	53	0.070	0.471
Fettnuss	91	2.997	0.732
Genesee	53	0.457	2.479
Gottelborn	59	0.077	0.286
Gottelborn < 150	99	7.013	0.842
Kellingley 45	90	1.070	0.254
Kellingly coarse	48	0.073	0.531
Kleinkopje	56	0.056	0.249
Kleinkopje	99	1.612	0.167
Middelburg fine	62	0.103	0.275
Polish	59	0.112	0.349
Polish	85	1.038	0.394
Polish	90	1.103	0.249
Polish 5600	54	0.149	0.968
South African	68	0.332	0.564
Spitsbergen	62	0.277	0.747

[a]Activation energy, E_a, (kJ/mol) and pre-exponential factor, A_a,(g/m^{2}sPa). A_{74} is the determined pre-exponential factor with a constant apparent activation energy of 74 kJ/mol

Table 4.
Parent coals, kinetic parameters of chars, apparent reaction orders of chars.

Coal	E_a [a]	A_a [a]	n_{opt} [a]
1. Anthracite	113	0.00823	0.95
2. Charbon Vietnamien	43	0.055	0
3. Charbon Chinois	83	2.72	0
4. Niederberg	85	2.01	0
5. Silo Sample	95	0.202	0.38
1. Beach tree	33	0.00025	0.78

[a]Apparent activation energy (kJ/mol), apparent pre-exponential factor (kg/m^2sPa^n) and the apparent reaction order *n*

5.1.3 Comparing reaction orders of anthracite chars and bituminous coal chars

Fig. 31 displays *F* for 10 bituminous coal chars, the 5 anthracite chars and $f_{\min}$ for the single biomass char as a function of *n*. While the optimum *n* is around one for the bituminous coal chars, the optimum *n* for the anthracite chars is zero.

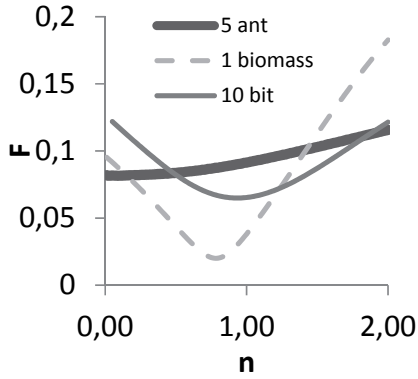

Fig. 31. Mean objective function as a function of the apparent reaction order for 5 anthracite chars and for 10 bituminous coal chars, and the objective function of one biomass char.

Fig. 32 shows modeled and experimental burnout profiles of one anthracite char, the biomass char, and one bituminous coal char. The initial mean sizes of the anthracite char, biomass char, and the bituminous coal char are similar: 39 µm, 41 µm, and 42 µm, respectively. The figure shows good agreement between modeled and experimental char oxidation rates to around 70% of char conversion. The figure shows remarkable rate differences between the three categories of chars. At 1673 K and 4 vol.% O_2, the time to 50% conversion of the biomass char is around 100 ms, while the corresponding time for the bituminous coal char and anthracite char is around 200

ms and 500 ms, respectively. At 1223 K and 4 vol.% O_2, the time to 50% conversion of the biomass char is around 150 ms, while the time of the bituminous coal char is around 1000 ms. The anthracite char reaches only around 15% of conversion in the IPFR in the investigate time interval.

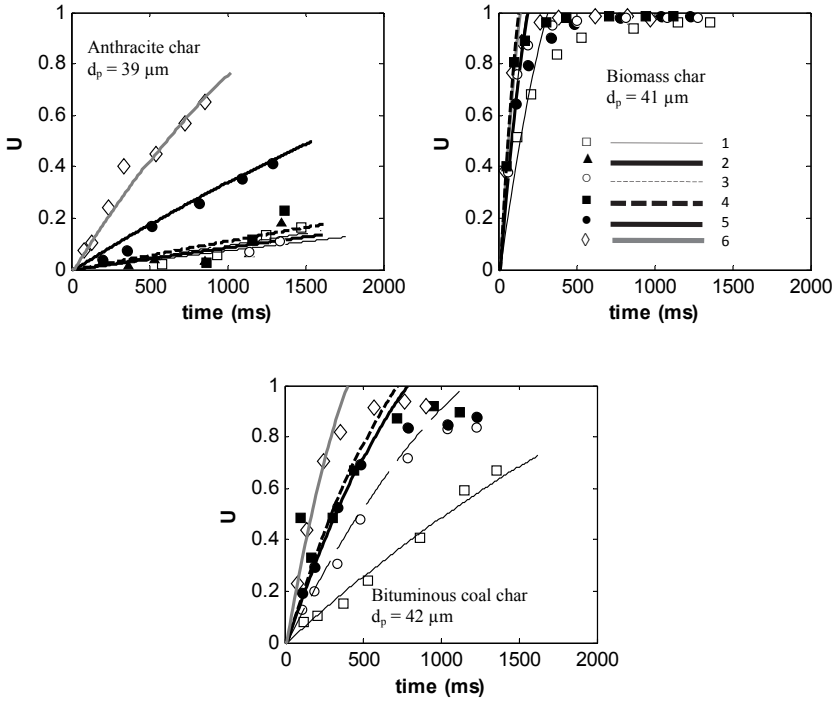

Fig. 32. Burnout profiles of one anthracite char, and one biomass char and one bituminous coal char. Symbols refer to experiments and lines refer to modeling. The conditions in the surrounding gas are (T (K)/vol.% O_2): (1) 1223/4, (2) 1223/6, (3) 1223/8, (4) 1223/12, (5) 1473/4, and (6) 1673/4.

The maximum values of the modeled particle temperatures are shown in Fig. 33. At the gas temperature of 1673 K, the maximum particle temperatures of the anthracite char, biomass char, and the bituminous coal char are 1688 K, 1853 K, and 1737 K. At 1223 K, the corresponding particle temperatures are 1225 K, 1270 K, and 1229 K. Regarding the high particle temperatures, especially for the biomass char at 1673 K, it is useful to compare experimental char-C oxidation rates to rates controlled by external diffusion. The maximum values of these rate fractions are shown in Fig. 34 for the three chars. The highest value can be observed for the biomass char, i.e., 0.12. Thus it is obvious that the char-C oxidation does not occur under Regime III conditions.

The char oxidation rates are so slow for the anthracite char, i.e., the fraction < 0.005, that the oxidation may take place under Regime I conditions. This could explain a reaction order of zero which is hard to justify under Regime II conditions. If Regime II conditions would occur, the entire internal surface area would not be active in the heterogeneous reactions. Therefore an increased concentration of reactants must give a higher oxidation rate, though the reaction order of the rate limiting step is zero.

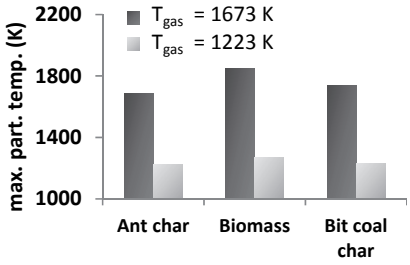

Fig. 33. Maximum modeled temperature of ~40 µm anthracite char particle, biomass char particle, and bituminous coal char particle at 1223 K or 1673 K with 4 vol.% O_2.

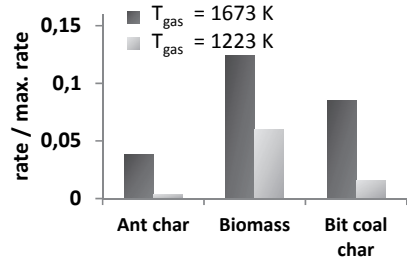

Fig. 34. Maximum value of oxidation rate divided by rate controlled by external diffusion of ~40 µm anthracite char particle, biomass char particle, and bituminous coal char particle at 1223 K or 1673 K with 4 vol.% O_2.

Fig. 32 shows that as the oxygen concentration increases from 4 to 12 vol.% O_2, the combustion rate changes negligibly for the anthracite char, while it changes significantly for the bituminous char: at 4 vol.% O_2 and 1473 K, the oxidation rate is lower than at 12 vol.% O_2 and 1223 K. However, for the anthracite char, the oxidation rate at 4 vol.% O_2 and 1473 K is significantly higher than at 1223 K and 12 vol.% O_2. One explanation for this deviation could lie in differences in particle temperatures, but, as discussed above, the temperatures of the anthracite

char particles and the bituminous coal char particles do not differ sufficiently from each other to justify such a deviation. Moreover in both cases the effects of external diffusion are relatively small and cannot explain the observed difference. Therefore is likely that not only the overall oxygen pressure dependence on the reaction rate, but also the true limiting reaction order, are different for the bituminous coal chars and the anthracite chars at the investigated conditions: the true reaction order of the anthracite chars is low, i.e., close to zero, and the true reaction order of the bituminous coal chars is high, i.e., close to one.

Various char oxidation mechanisms have been presented in the literature to explain experimentally observed char oxidation behavior. Hurt and Calo [21] pointed out that most char oxidation mechanisms are too detailed for practical use. Therefore they proposed a semi-global mechanism:

$$2C(s) + O_2(g) \rightarrow 2C(O) \qquad \text{(R5)}$$

$$C(O) + O_2(g) \rightarrow CO/CO_2(g) \qquad \text{(R6)}$$

$$C(O) \rightarrow CO(g) \qquad \text{(R7)}$$

Here C(O) represents chemisorbed oxygen atoms at a carbon site. The objective of this model is a quantitative treatment, which requires simple forms of the corresponding rate laws. In R6 the reaction product can be either CO or CO_2 and, therefore, the reaction contains implicit free sites to balance elemental carbon on the left hand side. Hurt and Calo [21] emphasize that any of the three steps may be a lumped description of several elementary steps. From this mechanism, the overall rate can be expressed as:

$$r = k_6 P_{O_2} \theta + k_7 \theta \qquad (39)$$

where θ is the coverage of chemisorbed oxygen atomes and k_i is the kinetic rate constant. At a given temperature and oxygen partial pressure, the overall rate dependence on the partial pressure of oxygen is independent of the value of θ, i.e., the effective reaction order is constant. Since the oxidation rates of the anthracite chars are lower than of the bituminous coal chars, the intra-particle oxygen pressure is expected to be slightly higher for the anthracite chars than for the

bituminous coal chars. Following Eq. 39, the reaction order for the anthracite chars should be equal to or higher than the reaction order for the bituminous coal chars. This is in contrast to the observed difference between the two categories of chars. One possibility is, therefore, to introduce the following step:

$$2C(O) \rightarrow CO_2(g) + C(s) \qquad \text{(R8)}$$

This oxidation step has frequently been suggested as a possible reaction step in the oxidation of chars [e.g. 13,20]. Taking into account this step, the overall oxidation rate becomes

$$r = k_6 P_{O_2} \theta + k_7 \theta + k_8 \theta^2 \qquad (40)$$

Assuming that $k_8 > k_6 p_{O_2}, k_7$ at the investigated temperatures, the overall rate is simplified to

$$r = k_8 \qquad (41)$$

as $\theta \rightarrow 1$. However for low values of θ the overall rate equals Eq. 39. Thus, as $\theta \rightarrow 1$, the limiting reaction order approaches zero, and as $\theta \rightarrow 0$ the true reaction order is between zero and one, depending on the values of the kinetic parameters. For anthracite chars, the specific internal surface area is essentially inaccessible, since the initial specific internal surface area of the parent coal is low, and remains so, since effects of devolatilization on the internal surface area are small [3]. For bituminous coals, the pores open up to a much higher extent during devolatilization due to the higher volatile content [3]. Therefore it is possible that the coverage of chemisorbed oxygen atoms is locally higher for the anthracite chars than for the bituminous coal chars at the investigated temperature. This is also supported by the numerical results by Geier et al. [10]. They showed with a similar model as presented here (the model of this study and the model by Geier et al. [10] were presented at the 34th Symposium (International) on combustion) that by slightly increasing the oxygen pressure at temperatures of around 1200 K, the coverage of chemisorbed oxygen atoms can increase significantly. Since the burning rates of the anthracite chars is slower than those of the bituminous coal chars, the oxygen pressure inside the anthracite

chars is expected to be higher than for the bituminous coal chars. In such a case, R8 plays a more important role for the anthracite chars, and the reaction order can be expected to be lower than for the bituminous coal chars. With R8 as the primary oxidation step, CO_2 is the primary oxidation product. As pointed out earlier, it has been suggested that CO is the major oxidation product at these temperatures [10,59]. The CO/CO_2 ratio increases partly due to intra-particle CO_2 reduction to CO. At the investigated temperature such reduction effects cannot be expected to be large following Stanmore et al. [64]. Therefore it is more likely that R8 in combination with R6 or R7 is rate limiting, rather than R8 alone. Nevertheless, in both of these cases a lower reaction order can be achieved for the anthracite chars than for the bituminous coal chars at the investigated temperatures. As a consequence, the difference in reaction orders between the anthracite chars and bituminous coal chars can be explained by the semi-global kinetic model [21] by also considering the additional step $2C(O) \rightarrow CO_2 + C$ in the char oxidation.

5.2 Char-N oxidation

In this thesis three NO release model during char oxidation are investigated: the numerical model presented in Chapter 4.2.1, the analytical model presented in Chapter 4.2.2 and the simplified model based on apparent kinetics presented in Chapter 4.2.3. In Chapter 5.2.1, results are presented from the numerical and analytical model. In Chapter 5.2.2, results from the simplified model based on apparent kinetics are presented.

5.2.1 Numerical and analytical model

The numerical NO release model has been tested for single char particles of spruce bark. The determined parameters are available in Table 5. For the NO reduction, the activation energy is 71 kJ/mol and the reaction order is 0.59. Generally reaction orders for NO reduction inside biomass chars have been reported to be below one [44,51-55].

Fig. 35 shows modeled and experimental NO release rates at 1173 K and 10 vol.% O_2 using the numerical model. In the figure the NO release curves are in good agreement. Initially the NO release rates are low and then increase as a function of burnout.

Table 5.
Kinetic parameters and reaction order for NO reduction of spruce bark char.

A_{i,O_2} [a]	$5.27 \cdot 10^{14}$
E_{i,O_2} [b]	168
$A_{i,NO}$	$2.38 \cdot 10^{4}$
$E_{i,NO}$	71
γ [c]	0.59

[a]Pre-exponential factor ((1/s(mol/m^3)$^\gamma$)
[b]Activation energy (kJ/mol)
[c]Reaction order

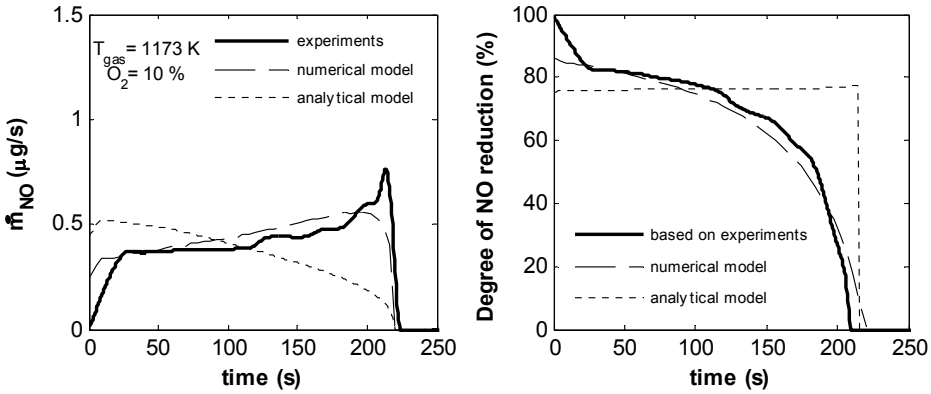

Fig. 35. Modeled and experimental NO release rates for char particles of spruce bark and degree of NO reduction inside particle. The initial diameter of the parent fuel particle was 0.8 cm.

In the figure, the modeled and experimentally based NO reduction degree (1-z) as a function of char oxidation time is also shown. Initially, the degree of NO reduction is close to 100% (z = 0) and, therefore, the NO release is low. The degree of NO reduction then decreases as a function of conversion and, correspondingly, the fractional conversion of char-N to NO increases. To compare the concentrations of NO inside and outside the particle, two points are selected from Fig. 35: A is at 50 seconds and B is at 190 seconds. From Fig. 35 it can be seen that the fractional conversion of char-N to NO is 20% at A and 60% at B. Fig. 36 displays the concentration of NO inside the char particle and outside the particle at points A and B. It can be seen that the absolute values of the NO concentration are significantly higher at point B than at point A inside the particle. This may be expected since the fractional conversion of char-N to NO is higher at A

than at B: the higher the fractional conversion of char-N to NO, the lower the concentration of NO inside the particle. Goel et al. [43] suggested that the char-N conversion is dependent upon the outflowing NO in such way that a steeper concentration gradient in the boundary layer favors NO diffusion from the particle, resulting in less reduction of NO. This is supported by the curves in Fig. 36: the NO concentration gradient outside the particle is much steeper for the smaller particle size. Thus, as the particle decreases in size the formed NO is more rapidly transported away from the particle and, consequently, less NO is reduced. Fig. 37 shows dimensionless radius, external surface area, and volume of the char core as functions of time at 1173 K and 10 vol.% O_2. In the figure the NO reduction degree curve is also plotted. In general, there is a relatively good agreement between the changes in radius and the changes in degree of NO reduction. This is equivalent to that the relationship - reduction of NO/formation of NO - is approximately proportional to the diameter of the char particle.¨

It is likely that the NO concentration inside the particle increases as a function of conversion. One interesting point is that the lower the reaction order, the less the NO reduction rate is influenced by an increased concentration of NO inside the particle. Thus, if the reaction order were, e.g., one, the fractional conversion of char-N to NO would not be increasing as rapidly as can be seen in Fig. 35 with a reaction order of 0.59. Two possible explanations may explain a higher reaction order than 0.59 (i) accumulation of nitrogen in the char [36,65,66] and (ii) thermal annealing [46]. (i) If nitrogen were retained in the char during the char oxidation, the initial formation rate of NO would be expected to increase and, moreover, the fractional conversion of char-N to NO would be expected to increase as a function of conversion. (ii) If thermal annealing occurs, the char reactivity for the NO reduction would be expected to decrease, resulting in a higher relative NO release rate as a function of conversion. Since these factors are not taken into account in the model, this may be compensated for by a reduced value in the reaction order.

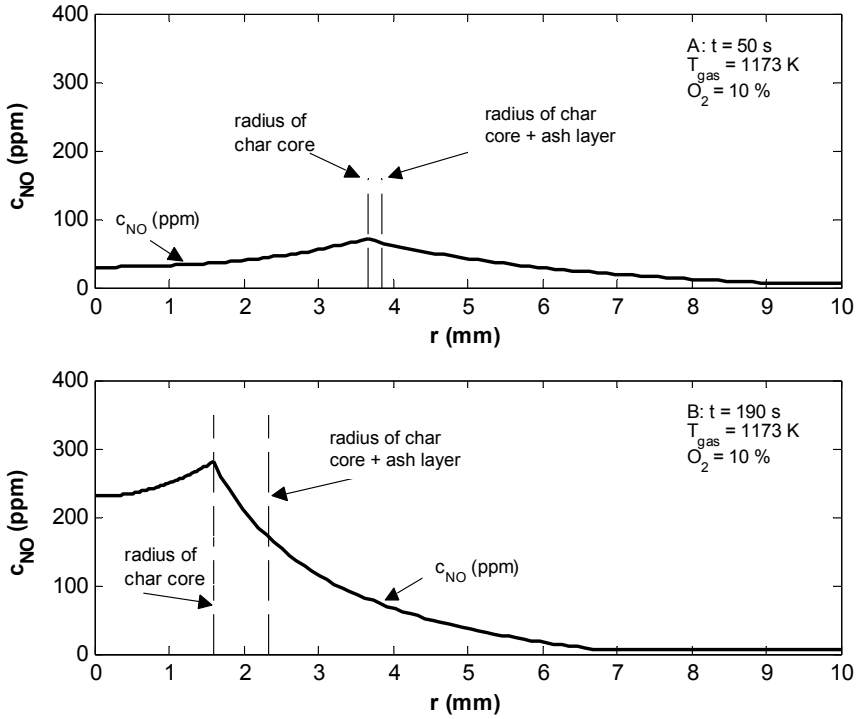

Fig. 36. Modeled NO concentration profiles inside and outside a biomass char particle.

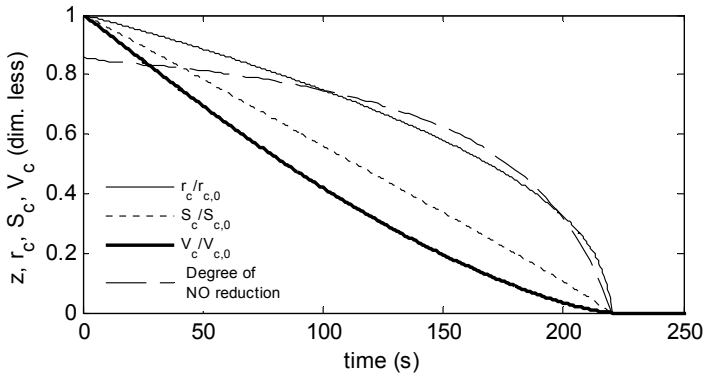

Fig. 37. Degree of NO reduction inside char particle (*z*), normalized particle diameter, external surface area, and volume as a function of time.

Fig. 38 shows modeled and experimental NO release rates at 1073 K and 1323 K with 10 vol.% O_2 by using the numerical model. At both temperatures the agreements are generally good. In both cases, there is a deviation between the curves during the initial char oxidation. During the first seconds of the char oxidation the NO release is close to zero according to the experiments. This cannot be seen in the modeled NO release curves. Garijo et al.[53] also observed this behavior during NO reduction experiments inside char particles of biomass. Their explanation is that the initially available NO is adsorbed onto the internal surface of the char and after a few seconds a steady state is reached between adsorption and desorption products. It is possible that this initial NO adsorption occurs in the experiments of this study. Nevertheless, since this has a small impact on the overall modeled NO release rates it is not included in the model. Fig. 39 shows modeled and experimental amount of nitrogen released from the char particle of NO. At 1073 K around 40% of the char-N is released as NO and at 1373 K around 20% of the char-N is released as NO.

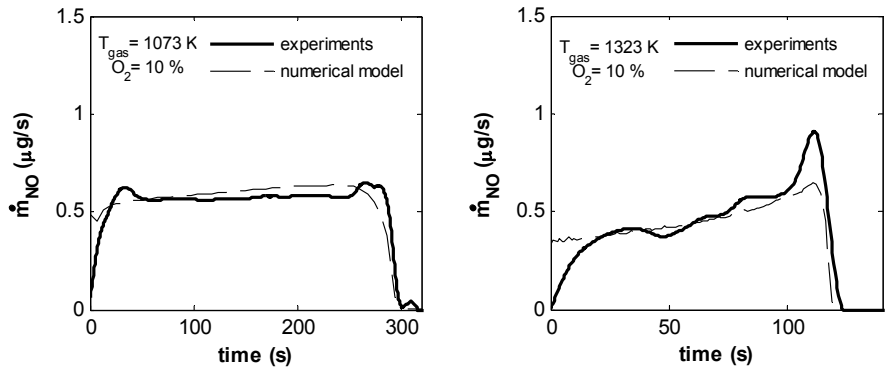

Fig. 38. Modeled and experimental NO release rates for char particles of spruce bark. The initial diameter of the parent fuel particle was 0.8 cm.

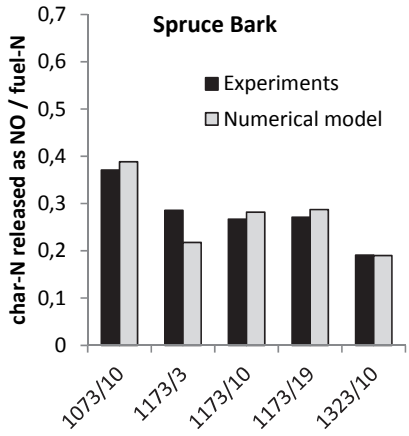

Fig. 39. Modeled and experimentally measured amount of NO released during char combustion of biomass particles. The numbers on the x-axes refer to temperature (K) and vol.% O_2 in the surrounding gas.

In the analytical model, the reaction order for the NO reduction is one and, therefore, the pre-exponential factor and the activation energy also differ [18] and must be determined separately. The activation energy for the NO reduction is in this case 200 kJ/mol and higher than for the numerical model and reported values in the literature [44,51-55]. Fig. 35 shows modeled and experimental NO release rates from a single biomass char particle at 1173 K and 10 vol.% O_2 by using the analytical model. It can be seen that the experimental NO release rate increases as a function of conversion, while the modeled NO release rate decreases as a function of conversion. Fig. 35 also shows modeled and experimentally based curves for the degree of NO reduction as a function of char oxidation time. The modeled degree of NO reduction is relatively constant as function of time by using the analytical model. In Fig. 36 it can be seen that the NO concentration is at its maximum at the external surface of the particle. Consequently, it is clear that the assumption of the analytical model that the concentration of NO is zero at the external surface area of the particle is insufficient for the experiments investigated in this study.

The kinetic parameters were determined from the experiments shown in Fig. 35 and Fig. 38 and also from the other experiments as described in the experimental section. To validate the numerical model, experiments were performed for larger particle sizes, i.e., initial mass of 0.5 g and diameter of 1 cm. Fig. 40 shows modeled and experimental NO release rates for these larger particles using the kinetic parameters determined for the smaller particles with an initial parent fuel diameter of 0.8 cm and mass of 0.2 g. These validation tests were performed at 1173 K with 10 and 19 vol.% O_2. At both conditions the agreement between the curves are good and the model is thus successfully validated for these conditions.

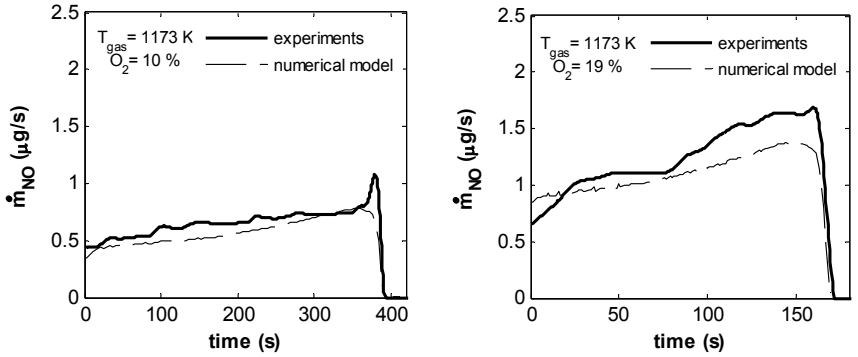

Fig. 40. Modeled and experimental NO release rates for char particles of spruce bark. The initial diameter of the parent fuel particle was 1 cm.

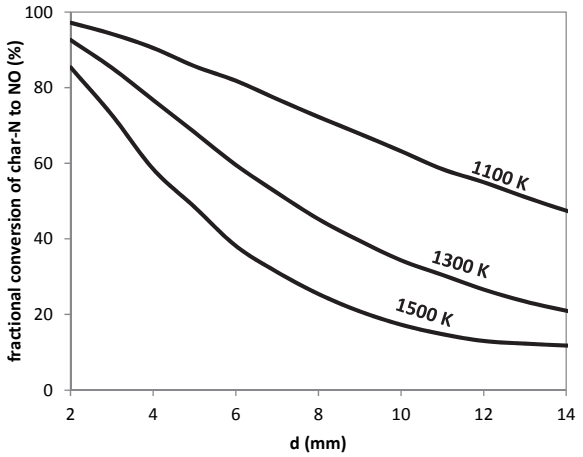

Fig. 41. Fractional conversion of char-N to NO as a function of particle diameter, and for various particle temperatures.

Fig. 41 shows calculated fractional conversion of char-N to NO as a function of particle size for various temperatures with a slip velocity of 0.15 m/s and with 10 vol.% O_2 in the gas. The figure illustrates that the fractional conversion of char-N to NO decreases as the temperature increases, for a given particle size. This may be explained by that the char-C oxidation is generally limited by external diffusion for the conditions considered in the figure. Thus, the initial formation rate of NO is also a function of external diffusion of oxygen and the NO formation rate increases slightly as the temperature increases. The NO reduction reactivity increases significantly, however, as a function of temperature and, therefore, more NO is reduced as the temperature increases.

Table 6.
Apparent kinetic parameters for NO reduction inside biomass char particles.

	$E_{a,NO}$ [a]	$A_{a,NO}$ [b]	n [c]
spruce bark	41	1.94E-5	0.90
SRC (poplar)	41	7.89E-6	0.85
straw	43	2.25E-5	0.70
torrefied wood	50	2.04E-5	1.00

[a]Apparent pre-exponential factor (kg/sm^{2}Pa^n)
[b]Apparent activation energy (kJ/mol)
[c]Apparent reaction order

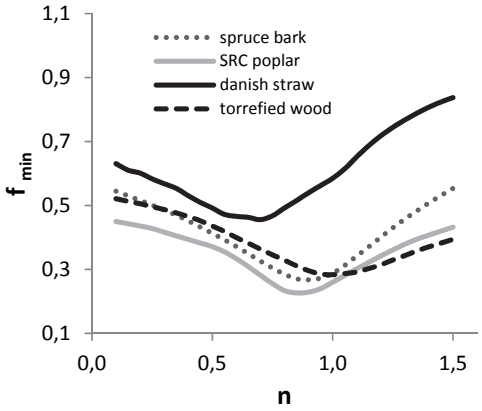

Fig. 42. Minimized objective function verses apparent reaction order for 4 biomass chars.

5.2.2 Apparent kinetics model

For the CFD applicable NO release model based on apparent kinetics, Fig. 42 shows minimized objective functions versus the reaction order for the 4 biomass chars. The values of the determined reaction orders and the corresponding kinetic parameters are given in Table 6. For the chars of spruce bark, SRC poplar, straw, and torrefied wood, the optimum reaction orders are 0.90, 0.85, 0.70, and 1.00, and the optimum apparent activation energies are 41, 31, 33, and 50 kJ/mol, which is in agreement with previously suggested values [44,51-55]. The activation energy for the spruce bark char was 71 kJ/mol in the numerical model, and the reaction order was 0.59. The deviation between the simplified model and the numerical model is expected, since in the numerical model the NO reduction rate is related to the true (calculated) concentration of NO inside the biomass char particle. Such "true" activation energy is higher than an apparent activation energy that incorporates diffusion effects such as in the simplified model based on apparent kinetics. Because of these effects, the apparent reaction order is expected to be higher than the "true" reaction order [11].

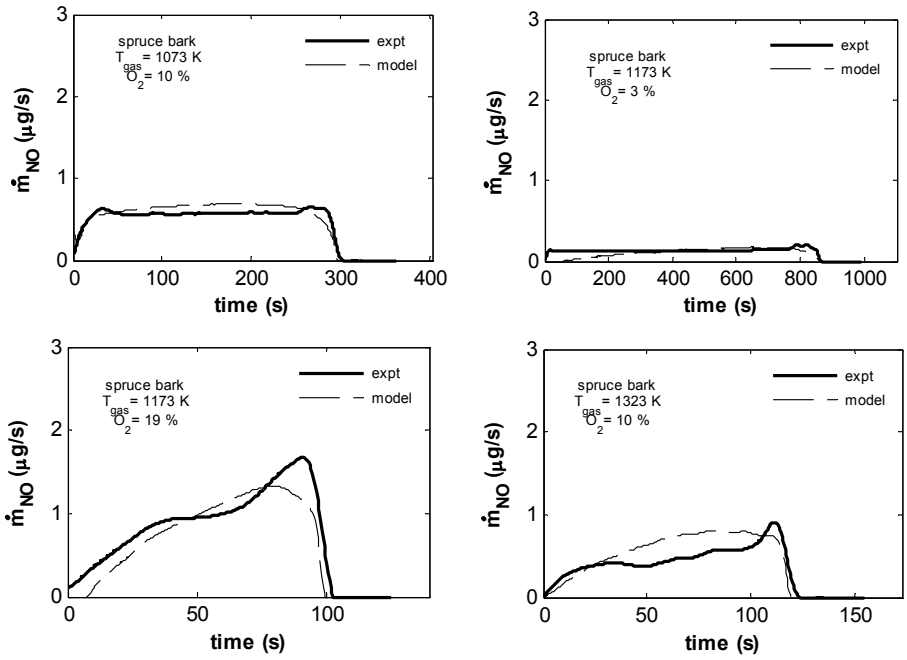

Fig. 43. Modeled and experimental NO release rates for char particles of spruce bark. The initial diameter of the parent fuel particle was 0.8 cm.

Fig. 43 shows modeled and experimental NO release rates of the spruce bark char at the following conditions (T_∞ (K)/O_2 (vol.%)): 1073/10, 1173/3, 1173/19, 1323/10. It can be seen that the NO release generally increases as a function of burnout. Fig. 44 shows modeled and experimental NO release rates of single char particles from spruce bark, SRC poplar, Danish straw and, torrefied wood at 1173 K and 10 vol.% O_2. Similarly as for the spruce bark char in Fig. 43, the modeled and the experimental NO release rates increase throughout the conversion. It can be seen in both figures that the modeled NO release in some cases starts at zero, while it sometimes starts at a higher value. This is because the entire formed NO is reduced according to the model.

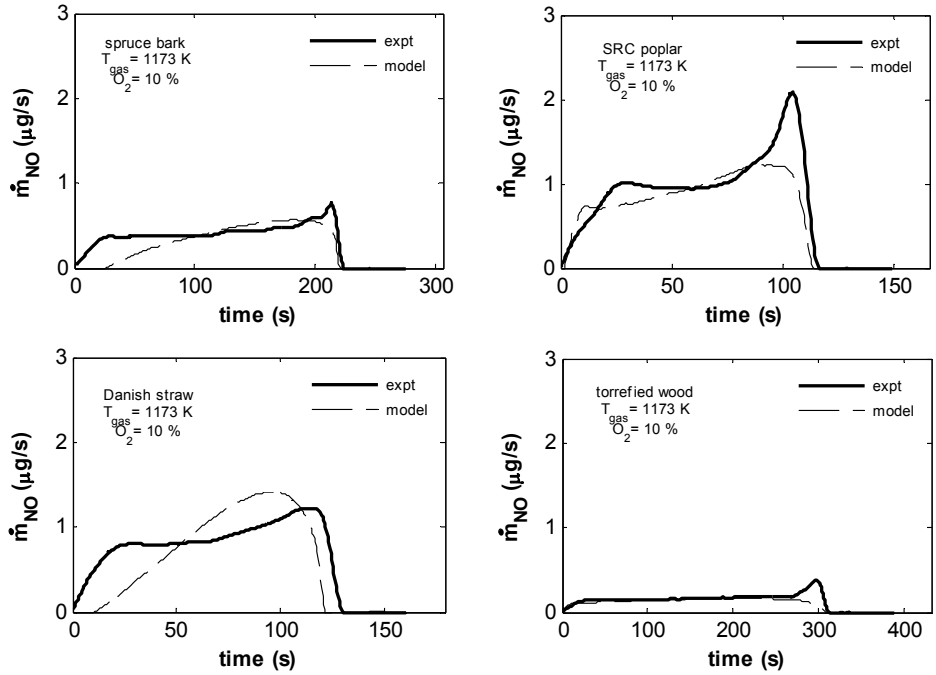

Fig. 44. Modeled and experimental NO release rates for char particles of spruce bark, SRC (poplar), straw, and torrefied wood. The initial diameter of the parent fuel particle was 0.8 cm.

Fig. 45 shows one example of the experimental NO release rate, and the estimated initial formation rate of NO, i.e., calculated from the measured carbon release rate and the measured nitrogen and carbon contents of the char. It can be seen that the initial formation rate of NO corresponds to the NO release rate at final conversion stages. This implies that none of the formed NO is reduced at these stages, and that the oxidation of carbon and nitrogen is entirely non-selective. Moreover this implies that nitrogen is not accumulated in the char during the char oxidation.

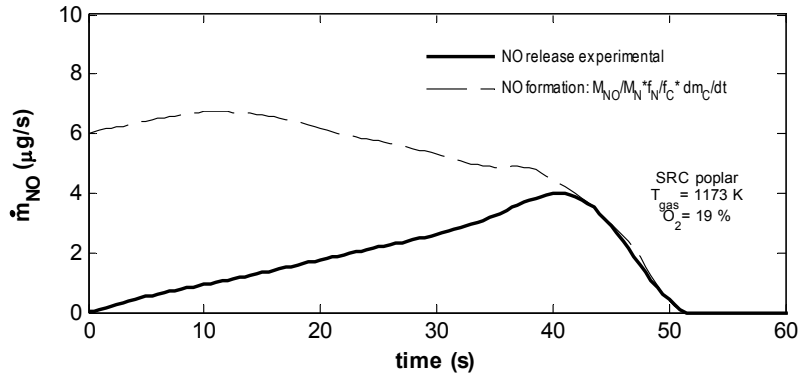

Fig. 45. Experimental NO release rate, and initial formation rate of NO as calculated from measured carbon release data of SRC poplar char particle at 1173 K and 19% O_2 in the surrounding gas. The initial diameter of the parent fuel particle was 0.8 cm.

Fig. 46 shows experimental and modeled amounts of released NO from the biomass chars. In all cases the agreement between the modeled and experimental amounts of released NO during the char combustion is good. At 1073 K and 10 vol.% O_2, the lowest value of the percentage of char-N being released as NO is observed for the Danish straw, 23%, and the highest value is observed for the torrefied wood char, 56%. At 1373 K and 10 vol.% O_2 the corresponding values are 15% (Danish straw char) and 24% (torrefied wood char). This is equivalent to that NO corresponding to 5–13% of the initial fuel-N nitrogen is released at 1073 K, and that NO corresponding to 3–5% of the initial fuel nitrogen is released at 1373 K during the char combustion stage. Based on these results, the Danish straw char has the best potential to reduce the formed NO, even though the potential is nearly as good for the other chars. Sørensen et al. [51] showed that the NO reduction potential for straw char is excellent at similar temperatures, as also investigated in this study. The values in Fig. 46 indicate that the char reactivity for NO reduction is nearly as good for the other

biomass chars. The values of the NO release in Fig. 46 are within the range of reported values. Winter et al. [39] combusted chars from five biomasses in a laboratory scale fluidized bed. They showed that 2–50% of the char-N is released as NO during the char conversion at 1073 K. Zheng et al. [67] concluded that NO corresponding to 10–20% of the initial fuel-N was released during char combustion of beech wood char at 973 K. Similar values were reported by Giuntoli et al. [68].

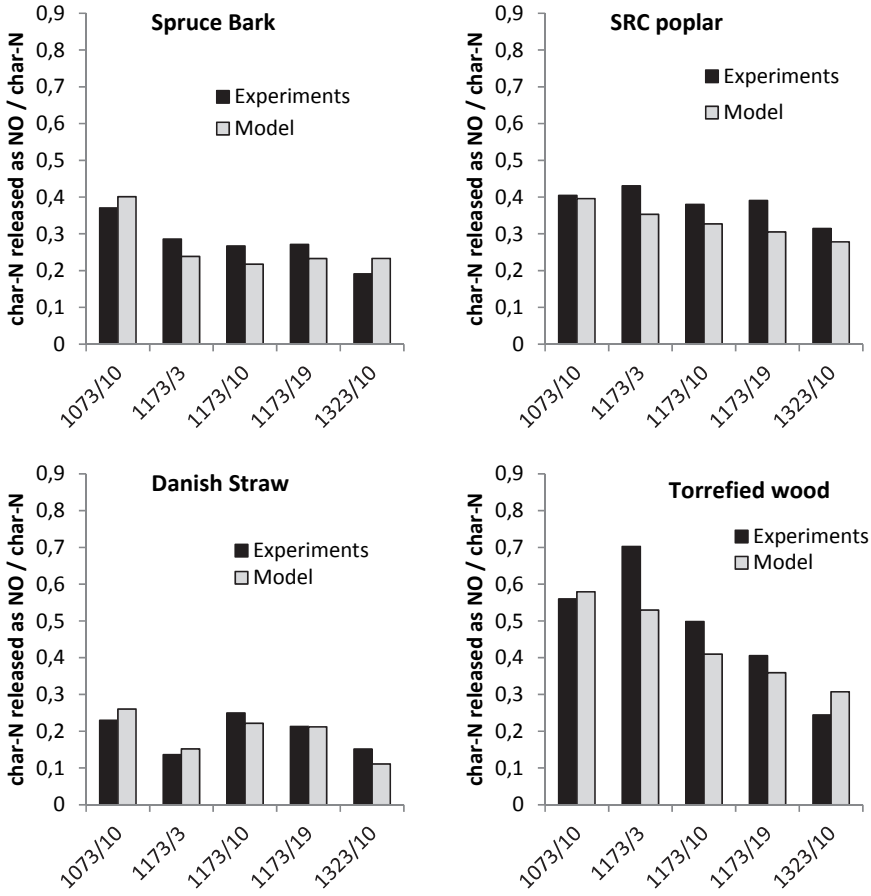

Fig. 46. Modeled and experimentally measured amount of NO released during char combustion of biomass particles. The numbers on the x-axes refer to temperature (K) and vol.% oxygen in the surrounding gas.

To validate the model, combustion experiments were performed in the SPR with larger particles of spruce bark and torrefied wood for 0.5 g particles such as in Fig. 40. Fig. 47 shows modeled and experimental NO release rates of these chars at 1173 K and with 10 and 19 vol.% O_2. In both cases, the agreement between the modeled and experimental NO release rates is good.

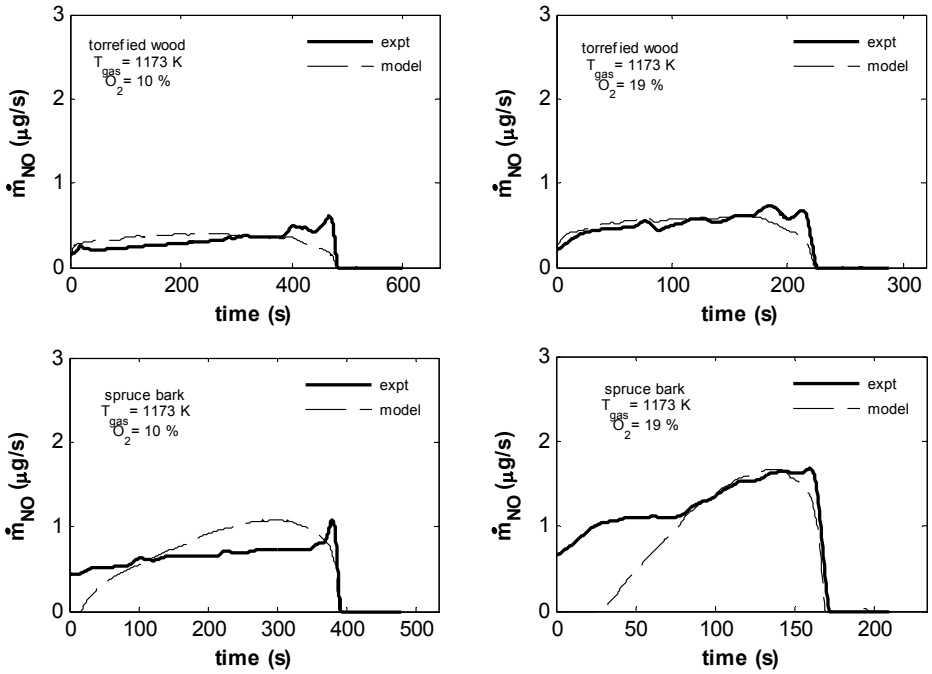

Fig. 47. Modeled and experimental NO release rates for char particles of torrefied wood and spruce bark. The initial diameter of the parent fuel particle was 1 cm.

Due to the large size of the char particles, the particle temperature is strongly influenced by radiation to and from the particle surface and of the energy produced/consumed in the char oxidation reactions. To test the sensitivity of the modeled NO release rates towards the particle temperature, the NO release rates have been modeled by assuming that (i) ε_p = 0.9, (ii) ε_p = 0.9 and H = 0.3 H, and (iii) H = 0.3 H. In the second and the third case, the reaction enthalpy is reduced to 30% of the reaction enthalpy used in the model. This corresponds to that CO would be the single reaction product. Fig. 48 shows modeled and experimental NO release rates of the SRC poplar char at 1073 K and 1323 K with 10 vol.% O_2 using the various parameter setups. It can be seen that the modeled NO release rates increase with increasing ε_p or with decreasing H. This can be explained by the particle temperature being lower in these cases compared to the original

case, and as a consequence the NO reduction rate decreases. Nevertheless, it can be seen that the accuracy of the modeled rates is not significantly reduced with the different approaches to model the particle temperature.

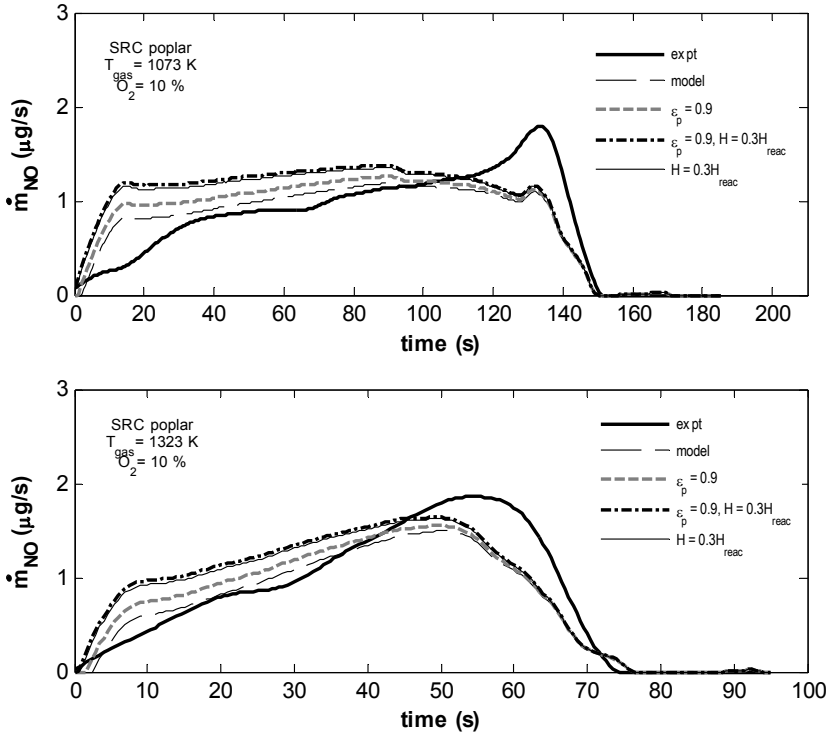

Fig. 48. Modeled and experimental NO release rates for SRC poplar char particle, using various parameter setups in the model. The initial diameter of the parent fuel particle was 0.8 cm.

6. Conclusions, implications and future work

6.1 Conclusions

For various types of solid fuel chars it was shown that a model based on apparent kinetics could be used to predict char-C oxidation from 0 to 70% of conversion under industrially relevant combustion conditions. The model requires only three fuel specific parameters – reaction order, apparent pre-exponential factor and activation energy – and can be incorporated as a sub-model for CFD modeling of char-C oxidation.

The results show that for a large number of bituminous coal chars both the apparent reaction order and the apparent activation energy can be assumed to be constant under conditions limited by the combined effects of chemical kinetics and pore diffusion. Thus, only one parameter, the pre-exponential factor, is required to predict char oxidation profiles. Based on this a new CFD applicable sub-model was developed. CFD modeling can be used to design new combustion systems. By using the new one-parameter model, the CFD modeling is significantly simplified since fewer fuel specific parameters are required.

The thesis show that under similar temperatures, oxygen concentrations and particle sizes, the apparent reaction orders for bituminous coal chars and anthracite chars differ; apparent reaction orders for bituminous coal chars were determined to be one while apparent reaction orders for anthracite chars were determined to be zero. This deviation in reaction orders has not previously been observed in the literature and should be considered in future char oxidation models. One of the most frequently used comprehensive char oxidation models could not explain the deviation in the reaction orders. In the thesis a modification to the model was suggested in order to explain the difference in reaction orders between anthracite chars and bituminous coal chars.

Two models were developed for the initial formation and reduction of NO during the oxidation of single biomass char particles. In both models that char-N is assumed to be oxidized to NO and the NO is partly reduced inside the particle. One of the models is based on the governing equations of NO inside and outside the particle and the second model is simplified to such extent that it is based on apparent kinetics and can be incorporated as a sub-model into a CFD code.

Modeled NO release rates from both models were in good agreement with experimental measurements from a single particle reactor.

6.2 Implications and future work

The developed char-C and char-N oxidation models of this thesis can be used to improve the combustion performance in various combustion devices or to develop completely new technologies. The CFD-applicable NO release model is the first of its kind and can be used to reduce NO emissions from combustion systems.

In this study it was shown that char-C oxidation rates with oxygen could be modeled with a constant activation energy and reaction order for bituminous coal chars. Moreover it was shown that reaction orders of anthracite chars and bituminous coal chars with respect to oxygen differ. Corresponding analyses should be performed for char oxidation by CO_2 and H_2O since these reactions plays an important role in many combustion systems. Moreover, CFD-applicable sub-models for the char oxidation by CO_2 and H_2O should be developed.

Future work should be done to test whether char-C oxidation models can be used to model late conversion stages without significantly increasing the number of parameters.

In this study, char-C oxidation tests were performed in an isothermal plug flow reactor. Similar comparative char-C oxidation studies should be performed using other experimental equipment such as in laminar flame reactors or laminar drop tube reactors.

The new NO release modeled developed in this thesis should be validated against experimental data in various kinds of laboratory scale combustion units. Finally, single particle char-C and char-N oxidation models should be incorporated into CFD codes, and validated against measured data from full scale combustion systems.

List of variables and parameters

A_a	Pre-exponential factor
A_i	Intrinsic pre-exponential factor
c	Concentration in ppm or vol.%
C	Molar concentration (mol/m^3)
d	Diameter (m)
D	Diffusion coefficient (m^2/s)
D	Diffusion rate coefficient (kg/m^{2}sPa)
E_a	Activation energy (J/mol)
f_h	Fraction of heat particle adsorbs
f_{min}	Objective function
F	Mean objective function
G	Constant for diffusion rate equation (kg/msPaK$^{0.75}$)
h	Convective heat transfer coefficient ($Nu/k{\cdot}d$)
H	Reaction enthalpy (J/kg)
I_μ	Confidence interval
k	Kinetic rate constant
k	Thermal conductivity (W/mK)
K	Mass transfer coefficient (m/s)
K	Kinetic rate constant
m	Mass (kg)
m	True reaction order
$\dot{m}$	Mass flow (kg/s)
M	Molar mass (kg/mol)
n	Apparent reaction order
n	Size of population
$\dot{n}$	Molar flow (mol/s)
N	Number of fuels
p	Pressure (Pa)
r	radius (m)
R	Universal gas constant (8.31 J/molK)
Re	Reynolds number
s_x	Standard deviation
S	External surface area (m^2)
Sc	Schmidt number
Sh	Sherwood number
t	Time (s)
t_α	t-quintile
T	Temperaure (K)
Th	Thiele modulus
u	Slip velocity (m/s)
U	Fractional degree of burnout

ν	Kinematic viscosity (m^2/s)	*a*	Apparent
$\dot{V}$	Volume flow (m^3/s)	*c*	Char particle
x	Molar fraction	*expt*	Experimental
$\overline{x}$	Mean value of population	*f*	Formation
Y	Mass fraction	*i*	Intrinsic
z	Fractional conversion of char-N to NO	*i*	NO and O_2
		j	Number of experiments
α	Burning mode	*k*	Number test conditions
γ	Reaction order	*N*	Number of fuels
δ	Boundary layer thickness (m)	*r*	Reduction
ε	Emissivity	*s*	External surface
ζ	Constant	∞	Gas phase
ρ	Density (kg/m^3)	*rad*	Raditation
σ	Stefan-Boltzmann constant ($5.67 \cdot 10^{-8}$ $Wm^{-2}K^{-4}$)	*0*	Initial

Subscripts

References

[1] http://www.iea.org/stats/ (accessed 4.1.2013)

[2] L. Kjäldman. Industrial Horizons, 1, 1994

[3] R.H. Essenhigh, Fundamentals of Coal Combustion, Chemisty of Coal Utilization, Elliot, 1981 (Chapter 19).

[4] A. Williams, J. M. Jones, L. Ma, M. Pourkashanian. Pollutants from the combustion of solid biomass fuels. Progress in Energy and Combustion Science, 38, 2012, 113-137

[5] A. Demirbas. Combustion characteristics of different biomass fuels. Progress in Energy and Combustion Science, 30, 2004, 219-230

[6] C. Di Blasi. Combustion and gasification rates of lignocellulosic chars. Progress in Energy and Combustion Science, 35, 2009, 121-140

[7] A. Williams, M. Pourjashanian, J. M. Jones. Combustion of pulverized coal and biomass. Progress in Energy and Combustion Science, 27, 2001, 587-610

[8] W. B. Fu, B. L. Zhang, S. M. Zheng. A relationship between the kinetic parameters of char combustion and the coal´s properties. Combustion and flame, 109, 1997, 587-598

[9] R. Phillips, F. J. Vastola, P. L. Walker Jr. Factors affecting the product ratio of the carbon-oxygen reaction-II- Reaction temperature. Carbon, 8, 1970, 205-210

[10] M. Geier, C. R. Shaddix, F. Holzleithner. A mechanistic char oxidation model consistent with observed CO2/CO product ratios. Proceedings of the Combustion Institute, 34, 2013, 2411-2418

[11] I. W. Smith. The combustion rates of coal chars: A review. 19th Symposium (International) on Combustion, 1982, 1045-1065

[12] P. L. Walker Jr., R. L. Taylor, J. M. Ranish. An update on the carbon oxygen reaction. Carbon, 29, 1991, 411-422

[13] R. E. Mitchell, L. Ma, B. Kim. On the burning behavior of pulverized coal chars. Combustion and Flame, 151, 2007, 426-436

[14] M. M. Baum, P. J. Street. Predicting the combustion behavior of coal particles. Combustion Science and Technology, 1971, 3, 231-243

[15] R. H. Hurt, R. E. Mitchell. Unified high-temperature char combustion kinetics for a suite of coals of various rank. 24th Symposium (International) on Combustion, 1992, 1243-1250

[16] R. H. Hurt, J.K. Sun, M. Lunden. A kinetic model of carbon burnout in pulverized coal combustion. Combustion and flame, 113, 1998, 181-197

[17] J. Ballester, S. Jiménez. Kinetic parameters for the oxidation of pulverized coal as measured from drop tube tests. Combustion and Flame, 142, 2005, 210-222

[18] J. J. Murphy, C. R. Shaddix. Combustion kinetics for coal chars in oxygen-enriched environments. Combustion and Flame, 144, 2006, 710-729

[19] L. Kurylko, R. H. Essenhigh. Steady and unsteady combustion of carbon. 14th Symposium (International) on Combustion, 1973, 1375-1386

[20] E. M. Suuberg, M. Wójtowicz, J. M. Calo. Reaction order for low temperature oxidation of carbons. 22nd Symposium (International) on Combustion, 1988, 79-87

[21] R. H. Hurt, J. M. Calo. Semi-global intrinsic kinetics for char combustion modeling. Combustion and flame, 125, 2001, 1138-1149

[22] M. A. Field. Measurements of the effect of rank on combustion rates of pulverized coal. Combustion and flame, 14, 1970, 237-248

[23] I. W. Smith. Kinetics of combustion of size-graded pulverized fuels in the temperature range 1200-2270 K. Combustion and flame, 17, 1971, 303-314

[24] H. Haykiri, A. Ersoy-Mericoyu, S. Kucubayrak. Effect of mineral matter on the reactivity of lignite chars. Energy Conversion and Management, 42, 2000, 11-20

[25] T. Lang, R. H. Hurt. Char combustion reactivities for a suite of diverse solid fuels and char-forming organic model compounds. Proceedings of the Combustion Institute, 29, 2002, 423-431

[26] M. F. R. Mulcahy, I. W. Smith. Kinetics of combustion of pulverized fuel: a review of theory and experiment. Review of pure and applied chemistry, 19, 1969, 81-108

[27] O. Levenspiel. The Chemical Reactor Omnibook. Oregon State University Bookstores: Corvallis, OR, 1996

[28] A. Williams, M. Pourkashanian, J. M. Jones. The combustion of coal and some other solid fuels. Proceedings of the Combustion Institute, 28, 2000, 2141-2162

[29] G. Hargrave, M. Pourkashanian, A. Williams. The combustion and gasification of coke and coal chars. 21st Symposium (International) on combustion, 1986, 221-230

[30] W. F. Wells, S. K. Kramer, D. Smooth. Reactivity and combustion of coal chars. 20th Symposium (International) on combustion, 1984, 1539-1546

[31] M.-L. Chan, J. M. Jones, M. Pourkashanian, A. Williams. The oxidative reactivity of coal chars in relation to their structure. Fuel, 78, 1999, 1539-1552

[32] A. Molina, E. G. Eddings, D. W. Pershing, A. F. Sarofim. Char nitrogen conversion: implications to emissions from coal-fired utility boilers. Progress in Energy and Combustion Science, 26, 2000, 507-531

[33] Y. H. Song, J. M. Beer, A. F. Sarofim. Oxidation and devolatilization of nitrogen in coal char. Combustion Science and Technology, 28, 1982, 177-183

[34] G. G. De Soete. Heterogenous N_2O and NO formation from bound nitrogen atoms during coal char combustion. 23rd Symposium (International) on combustion, 1990, 1257-1264

[35] J. M. Jones, P. M. Patterson, M. Pourkashanian, A. Williams. Approaches to modelling heterogeneous char NO formation/destruction during pulverised coal combustion. Carbon, 37, 1999, 1545-1552

[36] P. J. Ashman, B. S. Haynes, A. N. Buckley, P. F. Nelson. The fate of char-nitrogen in low-temperature oxidation. 27th Symposium (International) on combustion, 1998, 3069-3075

[37] L. L. Baxter, R. E. Mitchell, T. H. Fletcher, R. H. Hurt. Nitrogen release during coal combustion. Energy and Fuels, 10, 1996, 188-196

[38] P. Glarborg, A. D. Jensen, J. E. Johnsson. Fuel nitrogen conversion in solid fuel systems. Progress in Energy and Combustion Science, 29, 2003, 89-113

[39] F. Winter, C. Wartha, H. Hofbauer. NO and N_2O formation during combustion of wood strawm, malt waste and peat. Bioresource Technology, 70, 1999, 39-49

[40] F. Winter, C. Wartha, C. Löffler, H. Hofbauer. The NO and N_2O formation mechanism during devolatilization and char combustion under fluidized-bed conditions. 26th Symposium (International) on combustion, 1996, 3325-3334

[41] C. J. Tullin, S. Goel, A. Morihara, A. Sarofim. Nitrogen oxide (NO and N2O) formation for coal combustion in a fluidized bed: effect of carbon conversion and bed temperature. Energy and Fuels, 7, 1993, 796-802

[42] G. X. Yue, F. Pereira, A. F. Sarofim, J. M. Beer. Char nitrogen conversion to NO_x in a fluidized bed. Combustion Science and Technology, 83, 1992, 245-256

[43] S. Goel, A. Morihara, C. J. Tullin, A. Sarofim. Effect of NO and O_2 concentration on N_2O formation during combustion in a fluidized-bed combustion: modeling results. 25th Symposium on (Int.) Combustion, 1994, 1051-1059

[44] R. Zevenhofen, M. Hupa. The reactivity of chars from coal, peat and wood towards NO, wich and without CO. Fuel, 77, 1998, 1169-1176

[45] I. Aarna, E. M. Suuberg. The role of carbon monoxide in the NO-carbon reaction. Energy and Fuels, 13, 1999, 1145-1153

[46] I. Aarna, E. M. Suuberg. A review of the kinetics of the nitric oxide-carbon reaction. Fuel, 76, 1997, 475-491

[47] J. O. L. Wendt. On the fate of fuel nitrogen during coal char combustion. AIChE Journal, 22, 1976, 102-110

[48] P. Kilpinen, S. Kallio, J. Konttinen, V. Barisic. Char-nitrogen oxidation under fluidised bed conditions: single particle studies. Fuel, 81, 2002, 2349-2362

[49] S. P. Visona, B. R. Stanmore. Modeling NO_x release from a single coal particle II. Formation of NO from char-nitrogen. Combustion and Flame, 106, 1996, 207-218

[50] S. P. Visona, B. R. Stanmore. Modeling nitric oxide formation in a drop tube furnace burning pulverized coal. Combustion and Flame, 118, 1999, 61-75

[51] C. O. Sørensen, J. E. Johnsson, A. Jensen. Reduction of NO over wheat straw char. Energy and Fuels, 15, 2001, 1359-1368

[52] X. Wang, J. Si, J. Tan, Q. Zhao, T. Xu. Kinetics investigation on the reduction of NO using straw char based on physicochemical characterization. Bioresource Technol, 102, 2011, 7401-7406

[53] E. Garijo, A.D Jensen, P. Glarborg. Kinetic study of NO reduction over biomass char under dynamic conditions. Energy and Fuels, 17, 2003, 1429-1436.

[54] L. Dong, S. Gao, W. Song, G. Xu. Experimental study of NO reduction over biomass char. Fuel Processing Technology, 88, 2007, 707-715

[55] M. Guerrero, A. Millera, M. U. Alzueta, R. Bilbao. Experimental and kinetic study at high temperatures of the NO reduction over Eucalyptus char produced at different heating rates. Energy and Fuels, 25, 2011, 1024-1033.

[56] J. J. Saastamoinen, R. Taipale. NO_x formation in grate combustion of wood. Clean Air, 4, 2003, 239-267.

[57] J. J. Saastamoinen, M. Huttunen, P. Kilpinen, L. Kjäldman, H. Oravainen, S. Bostrom. Emission formation during wood log combustion in fireplaces – part II: char combustion stage. Progress in Computational Fluid Dynamics, 6, 2006, 209-216

[58] V. V. Kalinchak, A. V. Dubinskii. Influence of Stefan flow on heat and mass transfer and kinetics of chemical reactions of a carbon particle in air. Journal of engineering physics and thermophysics, 68, 1995, 470-475

[59] L. Tognotti, J. P. Longwell, A. F. Sarofim. The products of the high temperature oxidation of a single char particle in an electrodynamic balance. 23rd Symposium (International) on combustion, 1991, 1207-1213.

[60] R. E. Mitchell, R. J. Kee, P. Glarborg, M. E. Coltrin. The effect of CO conversion in the boundary layer surrounding pulverized-coal char particles. 23rd Symposium (International) on combustion, 1991, 1169-1176

[61] H. Lu, W. Robert, G. Peirce, B. Ripa, L. L. Baxter. Comprehensive study of biomass particle combustion. Energy and fuels, 22, 2008, 2826-2839

[62] C. Chen, T. Kojima. Single particle combustion at moderate temperature: effects of ash. Fuel processing technology, 47, 1996, 215-232

[63] M. J. Groeneveld, W. P. M. van Swaaij. Gasification of char particles with CO_2 and H_2O. Chemical Engineering Science, 35, 1980, 307-313

[64] B.R. Stanmore, S.P. Visona. Combust. Flame, 113, 1998, 274-276

[65] P. J. Ashman, B. S. Haynes, P. M. Nicholis, P. F. Nelson. Interaction of gaseous NO with char during the low-temperature oxidation of coal chars. Proceedings of the Combustion Institute, 28, 2000, 2171-2179.

[66] P. Chambrion, T. Kyotani, A. Tomita. Role of N-containing surface specis on NO reduction by carbon. Energy and Fuels, 12,1998, 416-421.

[67] Y. Zheng, A. D. Jensen, P. Glarborg, K. Sendt, B. S. Haynes. Heterogeneous fixation of N_2: investigation of a novel mechanism for formation of NO. Proceedings of the Combustion Institute, 32, 2009, 1973-1980

[68] J. Giuntoli, W. de Jong, A. H. M. Verkoojien, P. Piotrowska, M. Zevenhoven, M. Hupa- Combustion characteristics of biomass residues and biowastes: fate of fuel nitrogen. Energy and Fuels, 24, 2010, 5309-5319

RECENT REPORTS FROM THE COMBUSTION AND MATERIALS CHEMISTRY GROUP OF THE ÅBO AKADEMI PROCESS CHEMISTRY CENTRE:

06-01	Edgardo Coda Zabetta	Gas-Phase Detailed Chemistry Kinetic Mechanism "ÅA". A Mechanism for Simulating Biomass Conversion Including Methanol and Nitrogen Pollutants -Validation, Verification and Parametric Tests
06-02	Mischa Theis	Interaction of Biomass Fly Ashes with Different Fouling Tendencies
06-03	Michal Glazer	TGA-Investigation of KCl-Kaolinite Interaction
07-01	Vesna Barišić	Catalytic Reactions of N_2O and NO over Bed Materials from Multi-fuel Circulating Fluidized Bed Combustion
07-02	Andrius Gudzinskas Johan Lindholm Patrik Yrjas	Sulfation of Solid KCl
07-03	Daniel Lindberg	Thermochemistry and Melting Properties of Alkali Salt Mixtures in Black Liquor Conversion Processes
07-04	Linda Fröberg	Factors Affecting Raw Glaze Properties
07-05	Tor Laurén	Methods and Instruments for Characterizing Deposit Buildup on Heat Exchangers in Combustion Plants
08-01	Erik Vedel	Predicting the Properties of Bioactive Glasses
08-02	Tarja Talonen	Chemical Equilibria of Heavy Metals in Waste Incineration -Comparison of Thermodynamic Databases-
08-03	Micaela Westén-Karlsson	Assessment of a Laboratory Method for Studying High Temperature Corrosion Caused by Alkali Salts
08-04	Zhang Di	*In vitro* Characterization of Bioactive Glass
08-05	Maria Zevenhoven, Mikko Hupa	The Environmental Impact and Cost Efficiency of Combustible Waste Utilization - The Potential and Difficulties of On-going Technology Developments
08-06	Johan Werkelin	Ash-forming Elements and their Chemical Forms in Woody Biomass Fuels
08-07	Hanna Arstila	Crystallization Characteristics of Bioactive Glasses
10-01	Markus Engblom	Modeling and Field Observations of Char Bed Processes in Black Liquor Recovery Boilers

RECENT REPORTS FROM THE COMBUSTION AND MATERIALS CHEMISTRY GROUP OF THE ÅBO AKADEMI PROCESS CHEMISTRY CENTRE:

11-01	Leena Varila *et al.*	Fyrtio År Oorganisk Kemi vid Åbo Akademi
11-02	Johan Lindholm	On Experimental Techniques for Testing Flame Retardants in Polymers
11-03	Minna Piispanen	Characterization of Functional Coatings on Ceramic Surfaces
11-04	Sonja Enestam	Corrosivity of Hot Flue Gases in the Fluidized Bed Combustion of Recovered Waste Wood
12-01	Xiaoju Wang	Enzyme Electrode Configurations: for Application in Biofuel Cells
12-02	Patrycja Piotrowska	Combustion Properties of Biomass Residues Rich in Phosphorus
12-03	Dorota Bankiewicz	Corrosion Behavior of Boiler Tube Materials during Combustion of Fuels Containing Zn and Pb
12-04	Mikael Bergelin, Jan-Erik Eriksson, Xiaoju Wang, Max Johansson,et al.	Printed Enzymatic Power Source with Embedded Capacitor on Next Generation Devices, Tekes-PEPSecond
12-05	Susanne Fagerlund	Understanding the in vitro dissolution rate of glasses with respect to future clinical applications

ISBN 978-952-12-2891-9

Åbo Akademi

9 789521 228919 >